

Interfacial supramolecular biomimetic epoxidation catalysed by cyclic dipeptides

Christopher Bérubé, Xavier Barbeau, Sébastien Cardinal, Pierre-Luc Boudreault, Corinne Bouchard, Nicolas Delcey, Patrick Lagüe & Normand Voyer

To cite this article: Christopher Bérubé, Xavier Barbeau, Sébastien Cardinal, Pierre-Luc Boudreault, Corinne Bouchard, Nicolas Delcey, Patrick Lagüe & Normand Voyer (2016): Interfacial supramolecular biomimetic epoxidation catalysed by cyclic dipeptides, *Supramolecular Chemistry*, DOI: [10.1080/10610278.2016.1236197](https://doi.org/10.1080/10610278.2016.1236197)

To link to this article: <http://dx.doi.org/10.1080/10610278.2016.1236197>

 [View supplementary material](#) 

 Published online: 13 Oct 2016.

 [Submit your article to this journal](#) 

 Article views: 35

 [View related articles](#) 

 [View Crossmark data](#) 

Interfacial supramolecular biomimetic epoxidation catalysed by cyclic dipeptides

Christopher Bérubé^a, Xavier Barbeau^b, Sébastien Cardinal^a, Pierre-Luc Boudreault^a, Corinne Bouchard^a, Nicolas Delcey^a, Patrick Lagüe^b and Normand Voyer^a

^aDépartement de Chimie and PROTEO, Université Laval, Québec, Canada; ^bDépartement de Biochimie, Microbiologie et Bioinformatique and PROTÉO, Université Laval, Québec, Canada

ABSTRACT

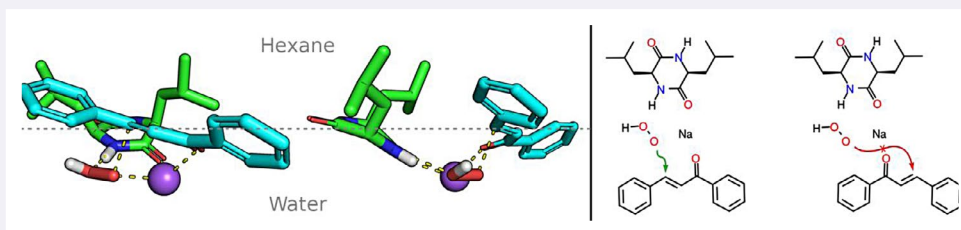
We synthesised a library of *cis*- and *trans*-cyclic dipeptides and evaluated their efficacy as catalysts in the asymmetric Weitz-Scheffer epoxidation of *trans*-chalcone. A thorough investigation relying on structure-activity studies and computational studies provided insights into the mechanism of the process. Our results revealed some structural features required for efficient conversion and for introduction of chirality into the product. The cyclic dipeptide acts as a catalyst by templating a supramolecular arrangement at the aqueous-organic interface required for efficient transformations to occur. Among all cyclic dipeptides investigated, *cyclo*(Leu-Leu) was the most efficient supramolecular catalyst.

ARTICLE HISTORY

Received 3 August 2016
Accepted 7 September 2016

KEYWORDS

Cyclic dipeptides; interfacial epoxidation; supramolecular catalysis



1. Introduction

Numerous reports describe the use of chiral receptors as chirality sources in chemical transformations. Although some efficient processes have been developed, most used the chiral receptors in stoichiometric amounts in organic solvents and the efficiency, in terms of yield, rate and enantioselectivity, is often moderate. The possibility of using chiral receptors as organocatalysts in greener solvents is highly desirable and has attracted considerable interest recently (1–4).

Notably, some supramolecular catalysts have been used successfully in aqueous media (5). Among those, cyclic dipeptides (CDPs) (which are 2,5-diketopiperazines), form supramolecular structures that could be useful in asymmetric catalysis (6–11). These compounds have well-oriented hydrogen bond donors and acceptors through their *cis*-amide functionality. Thus, CDPs form highly ordered supramolecular structures such as linear one-dimensional (1-D) hydrogen-bonded tapes and hydrogen-bonded dimers and multimers. Their properties could be exploited for efficient supramolecular chiral catalysis (12, 13). In

addition, *Cis* CDPs create a concave cavity that could serve as a receptor to bind a substrate in a chiral environment.

Along those lines, we recently reported the asymmetric epoxidation of α,β -unsaturated ketones in a triphasic system using insoluble CDPs located at the interface. Asymmetric epoxidation of a model substrate *trans*-chalcone (1) into epoxychalcone (2) using a catalytic amount of *cyclo*[Leu-Leu] (3a and 3b) led to 70% ee as described in Figure 1 (14). Interestingly, only a modest 15% ee was obtained when the linear L-Leucine dipeptide was used (15).

We wanted to develop more efficient supramolecular catalysts for asymmetric biomimetic epoxidation of a variety of α,β -unsaturated ketones, and to gain insights into the mechanism of the process. Therefore, we have prepared a library of CDPs and investigated their properties as supramolecular chiral catalysts. We also report modelling studies that aim at identifying the origin of the supramolecular catalysis. Our studies revealed some important supramolecular and structural features required for efficient conversion and more importantly, to create chiral products.

CONTACT Normand Voyer ✉ normand.voyer@chm.ulaval.ca

 Supplemental data for this article can be accessed here. [http://dx.doi.org/10.1080/10610278.2016.1236197]

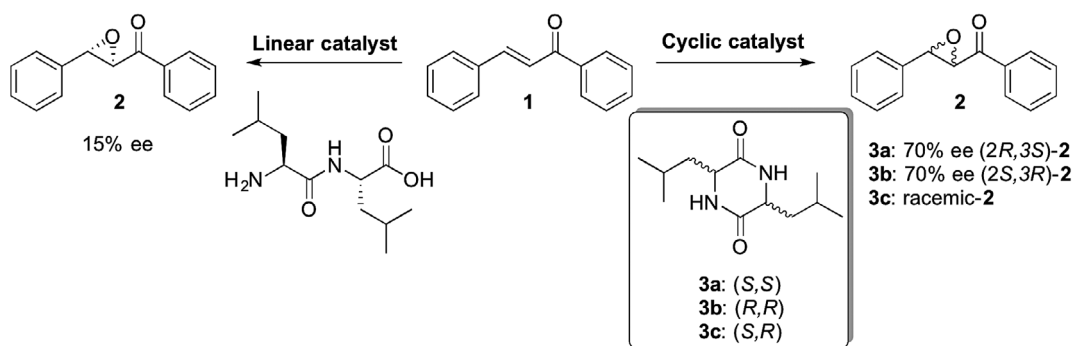


Figure 1. Catalyst rigidity effect in the asymmetric epoxidation of **1**.

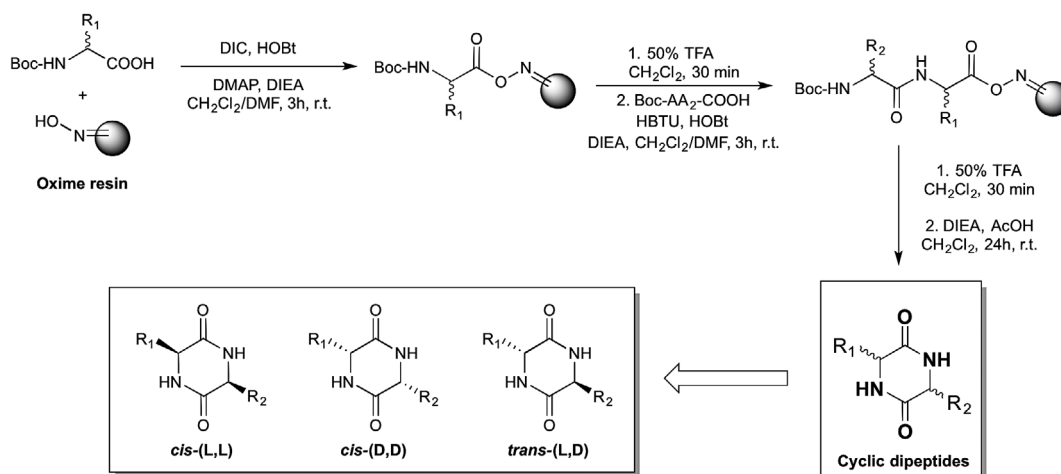


Figure 2. Synthetic strategy towards CDPs.

2. Results and discussion

2.1. Cyclic dipeptides synthesis

We synthesised a library of cyclic dipeptides with a variety of substituents and stereochemistries, by taking advantage of the availability of natural and synthetic amino acids to be chiral synthons. This library will facilitate the study of the structural features required for efficient conversion and enantioselectivity. Our synthetic procedure involves the condensation of two *N*-Boc amino acids using oxime resin (**16**, **17**) and standard peptide solid-phase synthetic strategies (Figure 2) (**18**).

Briefly, the first amino acid was coupled for three hours using diisopropylcarbodiimide (DIC) as coupling reagent. The *N*-Boc protecting group was removed using a mixture of 1:1 trifluoroacetic acid (TFA)/dichloromethane, while the second amino acid was activated with hydroxybenzotriazole (HOBt) and (2-(6-Chloro-1*H*-benzotriazole-1-yl)-1,1,3,3-tetramethylammonium hexafluorophosphate (HBTU). After deprotection, the linear dipeptide was simultaneously cyclised and cleaved from the resin in the presence of diisopropylethylamine (DIEA; 2.5 equiv) and acetic acid (AcOH; 5 equiv) in dichloromethane, leading

to high-purity CDPs **3–35**. Using the synthetic procedure described here, we successfully synthesised CDPs with a variety of chiral *cis* (Figures 3 and 4) and *trans* (Figure 5) side chains. Analogues with isopropyl, benzyl, dibenzyl, aliphatic, benzyloxymethyl groups and tricyclic derivatives have been prepared with high yields (>90%). A total of 58 CDPs were prepared and characterised by ¹H NMR, ¹³C NMR and mass spectrometry analyses. The procedure is robust and efficient, allowing the quick preparation of CDPs with purity sufficient to be used as-is, even on larger scales.

2.2. Evaluation of CDPs efficacy in the epoxidation of *trans*-chalcone

2.2.1. *cis*-(L,L) CDPs

As in a preliminary study (**14**), we chose *trans*-chalcone **1** as a model substrate for the present investigation. We used optimised conditions: 25% sodium hydroxide (NaOH) in hydrogen peroxide (30% H₂O₂) as an oxidant system, and 10 mol% of CDPs for 48 h at room temperature with hexanes as the organic phase (**14**). To evaluate the importance of the structure of CDPs on their catalytic efficiency,

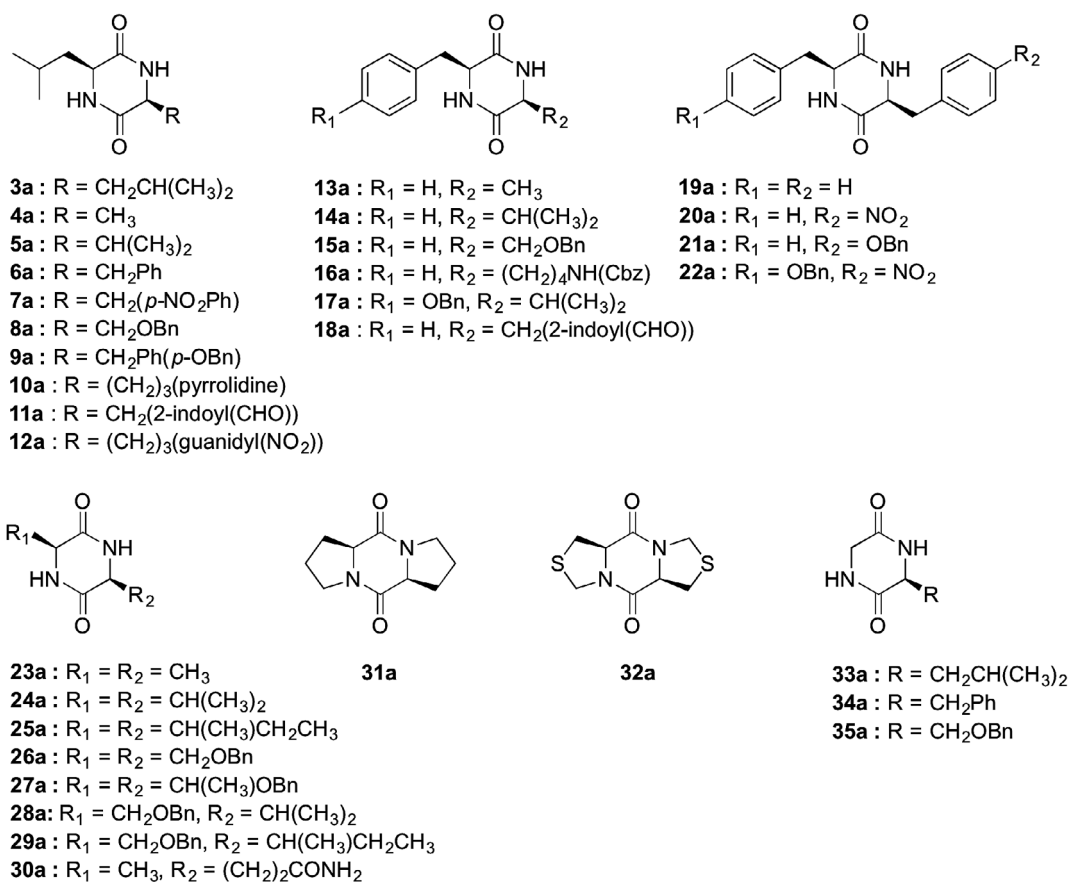


Figure 3. *cis*-(L,L) CDPs synthesised.

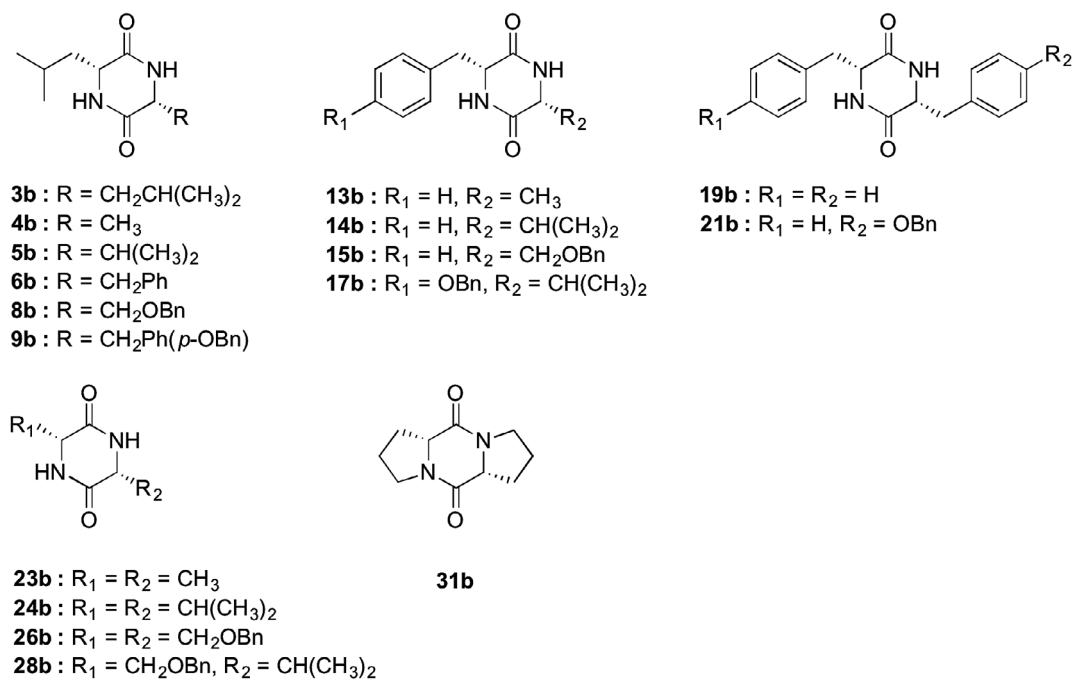


Figure 4. *cis*-(D,D) CDPs synthesised.

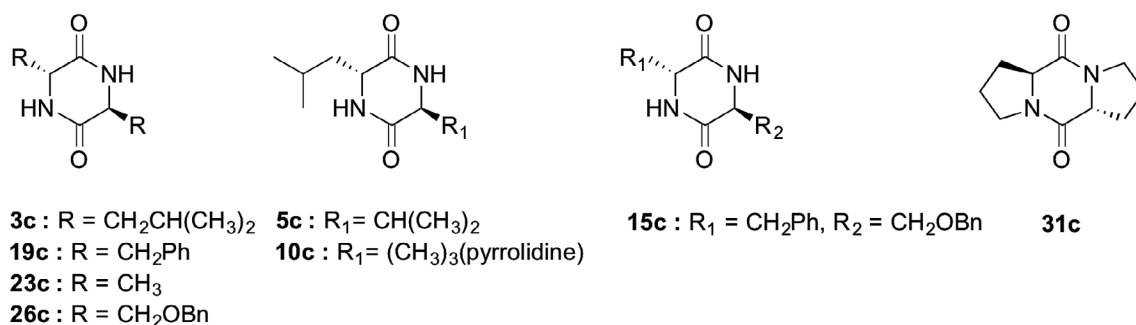


Figure 5. *trans*-(D,L) CDPs synthesised.

Table 1. Catalytic efficiency of *cis*-(L,L) CDP in the triphasic epoxidation of *trans*-chalcone 1.

Entry	Supramolecular catalyst	Conversion (%)	ee (%)
1	<i>cyclo</i> [L-Leu-L-Leu] 3a	33	70
2	<i>cyclo</i> [L-Leu-L-Ala] 4a	22	19
3	<i>cyclo</i> [L-Leu-L-Val] 5a	20	6
4	<i>cyclo</i> [L-Leu-L-Phe] 6a	19	9
5	<i>cyclo</i> [L-Leu-L-Phe(NO ₂)] 7a	26	0
6	<i>cyclo</i> [L-Leu-L-Ser(Bzl)] 8a	18	9
7	<i>cyclo</i> [L-Leu-L-Tyr(Bzl)] 9a	34	0
8	<i>cyclo</i> [L-Leu-L-Pro] 10a	26	50
9	<i>cyclo</i> [L-Leu-L-Trp(CHO)] 11a	30	0
10	<i>cyclo</i> [L-Leu-L-Arg(NO ₂)] 12a	44	28
11	<i>cyclo</i> [L-Phe-L-Ala] 13a	22	5
12	<i>cyclo</i> [L-Phe-L-Val] 14a	14	0
13	<i>cyclo</i> [L-Phe-L-Ser(Bzl)] 15a	22	0
14	<i>cyclo</i> [L-Phe-L-Lys(Z)] 16a	24	22
15	<i>cyclo</i> [L-Tyr(Bzl)-L-Val] 17a	18	0
16	<i>cyclo</i> [L-Phe-L-Trp(CHO)] 18a	25	0
17	<i>cyclo</i> [L-Phe-L-Phe] 19a	23	15
18	<i>cyclo</i> [L-Phe-L-Phe(NO ₂)] 20a	99	0
19	<i>cyclo</i> [L-Tyr(Bzl)-L-Phe] 21a	13	0
20	<i>cyclo</i> [L-Tyr(Bzl)-L-Phe(NO ₂)] 22a	24	0
21	<i>cyclo</i> [L-Ala-L-Ala] 23a	23	0
22	<i>cyclo</i> [L-Val-L-Val] 24a	20	5
23	<i>cyclo</i> [L-Ile-L-Ile] 25a	21	0
24	<i>cyclo</i> [L-Ser(Bzl)-L-Ser(Bzl)] 26a	22	6
25	<i>cyclo</i> [L-Thr(Bzl)-L-Thr(Bzl)] 27a	12	0
26	<i>cyclo</i> [L-Val-L-Ser(Bzl)] 28a	24	5
27	<i>cyclo</i> [L-Ile-L-Ser(Bzl)] 29a	22	0
28	<i>cyclo</i> [L-Ala-L-Gln] 30a	24	9
29	<i>cyclo</i> [L-Pro-L-Pro] 31a	19	0
30	<i>cyclo</i> [L-Thz-L-Thz] 32a	22	0
31	<i>cyclo</i> [Gly-L-Leu] 33a	18	0
32	<i>cyclo</i> [Gly-L-Phe] 34a	22	13
33	<i>cyclo</i> [Gly-L-Ser(Bzl)] 35a	18	0

we studied CDPs **3a-12a** that possess at least one isobutyl group (Table 1, entries 1–10). The model catalyst CDP **3a** led to 70% ee of (2*R*,3*S*)-epoxychalcone **2** (Table 1, entry 1). In all other cases, lower enantiomeric excesses were

obtained when the CDPs had other aliphatic side chains, such as methyl (**4a**) and isopropyl (**5a**), which led to 22% and 6% ee of (2*R*,3*S*)-epoxychalcone **2**, respectively (Table 1, entries 2 and 3).

CDP **6a**, with one benzyl side chain, provided **2** with only 9% ee (Table 1, entry 4). Interestingly, using CDP **7a**, which has an electron-withdrawing nitro group in the *para* position of the benzyl moiety of **6a**, provided racemic epoxychalcone with a slight increase in the conversion rate (Table 1, entry 5). Using CDPs bearing benzyloxymethyl (**8a**) and *p*-benzyloxybenzyl (**9a**) side chains led to 9% ee and racemic epoxide **2**, respectively (Table 1, entries 6 and 7). Good enantiomeric excess was obtained using CDP **10a** with a pyrrolidine side chain, with up to 50% ee of (*2R,3S*)-epoxychalcone **2** (Table 1, entry 8). The 2-indolyl carbaldehyde side chain CDP **11a** led to the racemic product (Table 1, entry 9). Using the nitroguanidine substituent of CDP **12a** improved the conversion to 44% and the enantiomeric excess up to 28% (Table 1, entry 10).

The results of these experiments demonstrate that the two isobutyl side chains are the best combination for higher yield and enantioselectivity. They also point out that very subtle changes lead to significant drops in efficiency. Clearly, the structure of the supramolecular complex relevant to catalysis involves more than just hydrophobic interactions at the interface and is not a simple phase transfer catalysis.

In a second series, we evaluated CDPs **13a–18a** with an isobutyl and a more hindered β -phenyl side chain (Table 1, entries 11–16). Catalyst **13a**, with a benzyl and a methyl side chain, provided (*2R,3S*)-epoxychalcone **2** with a low 5% ee (Table 1, entry 11). The analogues with one benzyl group and either an isopropyl (**14a**) or a benzyloxymethyl moiety (**15a**) led to racemic epoxychalcone in both cases (Table 1, entries 12 and 13). However, **16a** with a Cbz protected aminobutyl side chain was efficient to induce chirality to (*2R,3S*)-epoxychalcone **2** up to 22% ee (Table 1, entry 14). On the other hand, CDP (**17a**) with a *p*-benzyloxybenzyl and an isopropyl chiral side chains and CDP **18a** substituted by a benzyl and a 2-indolyl carbaldehyde led to racemic epoxide (Table 1, entries 15 and 16).

We also investigated CDPs **19a–22a**, which have two benzyl side chains with different functional groups in the *para* position. CDP **19a** provided 15% ee of (*2R,3S*)-epoxychalcone **2** (Table 1, entry 17). Compared to **19a**, using CDP **20a** with a *p*-nitro group on one phenyl moiety dramatically enhanced the reaction rate leading to quantitative conversion of racemic epoxychalcone **2** (Table 1, entry 18). In this case, the presence of the electron-withdrawing group seems to activate the substrate *trans*-chalcone **1**. Perhaps the nitro group on **20a** facilitates the formation of interfacial supramolecular complexes with **1**, which renders it more electrophilic and in close proximity to a hydroperoxide ion.

CDP with *p*-benzyloxybenzyl and benzyl substituents (**21a**) led to racemic epoxychalcone (Table 1, entry 19).

Considering previous results obtained with CDP **20a**, it was assumed that introducing a *p*-nitrobenzyl group in **22a** should enhance the reaction rate and induce chirality in the process. However, we obtained a low conversion rate and only 9% ee of (*2R,3S*)-epoxychalcone **2** (Table 1, entry 20).

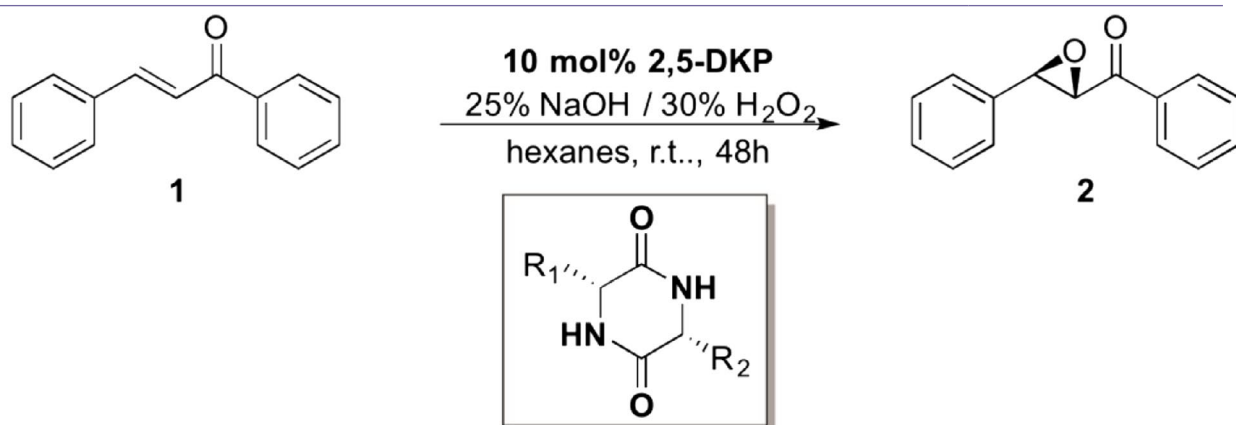
Further investigations were performed with CDPs that have two identical aliphatic side chains such as methyl (**23a**), isopropyl (**24a**) and *sec*-butyl (**25a**) (Table 1, entries 21–23). In all three cases, racemic epoxychalcone **2** was obtained in roughly 20% yields. These results are surprising, especially in the case of CDP **25a**, which has two *sec*-butyl side chains. Indeed, we observed a complete loss of enantioselectivity compared to CDP **3a** having two isobutyl groups from L-Leucine. Hence, it appears that β -substitutions on the side chains significantly affect the formation of a stable supramolecular complex between the CDP and the substrate. In the case of **23a** with a two methyl side chains, it is possible that the lower steric hindrance created by the CDP allows the formation of multiple supramolecular complexes yielding racemic epoxides.

We also evaluated CDPs with one or two benzyloxymethyl group side chains (**26a–29a**) (Table 1, entries 24–27). Only CDPs **26a** and **28a** produced epoxides with low enantiomeric excesses (6 and 5%, respectively) (Table 1, entries 24 and 26). Again, for a CDP with a β -substitution on the side chain, **27a**, a very low conversion and racemic epoxide **2** were obtained. These results further support the importance of the β -position for functional and efficient CDP catalysts. Introducing a hydrogen bond donor group into a CDP (**30a**) provided (*2R,3S*)-epoxychalcone **2** with only 9% ee (Table 1, entry 28). This result illustrates that the CDP side chains are involved in the enantioselectivity through steric interactions rather than through hydrogen bonding. On the other hand, tricyclic CDP **31a** (Table 1, entry 29) and its thio derivative **32a** (Table 1, entry 30) led to racemic epoxychalcone **2** in both cases.

Finally, with **33a–35a** we verified the efficiency of CDPs with only chiral side chains on the cyclic core (Table 1, entries 31–33). Interestingly, CDP with one isobutyl **33a** provided racemic epoxychalcone. The same result was obtained using **35a** with a benzyloxymethyl group. From that series, only CDP **34a** with a benzyl side chain led to low enantioselectivity (Table 1, entry 32).

In summary, these screening experiments showed that using *cis*-(L,L) CDPs led to the (*2R,3S*)-epoxychalcone enantiomer **2** in all cases. The best enantioselectivity was observed with CDPs with at least one isobutyl (leucine) side chain. Notably, the presence of a substituent at the β -position is highly detrimental to the enantioselectivity and efficiency. The best CDP catalyst **3a** has a C₂ symmetric

Table 2. Catalytic efficiency of *cis*-(D,D) CDP in the triphasic epoxidation of *trans*-chalcone **1**.

Entry	Supramolecular catalyst	Conversion (%)	ee (%)
			
1	<i>cyclo</i> [D-Leu-D-Leu] 3b	35	70
2	<i>cyclo</i> [D-Leu-D-Ala] 4b	23	17
3	<i>cyclo</i> [D-Leu-D-Val] 5b	17	6
4	<i>cyclo</i> [D-Leu-D-Phe] 6b	24	9
5	<i>cyclo</i> [D-Leu-D-Ser(Bzl)] 8b	21	8
6	<i>cyclo</i> [D-Leu-D-Tyr(Bzl)] 9b	30	0
7	<i>cyclo</i> [D-Phe-D-Ala] 13b	20	5
8	<i>cyclo</i> [D-Phe-D-Val] 14b	17	0
9	<i>cyclo</i> [D-Phe-D-Ser(Bzl)] 15b	17	0
10	<i>cyclo</i> [D-Tyr(Bzl)-D-Val] 17b	19	0
11	<i>cyclo</i> [D-Phe-D-Phe] 19b	21	10
12	<i>cyclo</i> [D-Tyr(Bzl)-D-Phe] 121b	17	0
13	<i>cyclo</i> [D-Ala-D-Ala] 23b	24	0
14	<i>cyclo</i> [D-Val-D-Val] 24b	23	5
15	<i>cyclo</i> [D-Ser(Bzl)-D-Ser(Bzl)] 26b	22	5
16	<i>cyclo</i> [D-Val-D-Ser(Bzl)] 28b	20	5
17	<i>cyclo</i> [D-Pro-D-Pro] 31b	18	0

structure. However, CDPs **23a–25a**, also C2 symmetric, are inefficient.

Overall, the above results illustrate that several parameters influence the formation of well-defined supramolecular complexes required for obtaining efficient enantioselective epoxidation of *trans*-chalcone (**1**) in high yields.

2.2.2. *cis*-(D,D) CDPs

To learn more about the mechanism and with the objective to access both enantiomers of epoxychalcone **2**, we evaluated *cis*-(D,D) CDPs in the asymmetric epoxidation of *trans*-chalcone **1**. For comparison with the *cis*-(L,L) CDPs described in Section 2.2.1, we synthesised the same CDPs starting from D-amino acids. Results are reported in Table 2. When tested in the same process under the same conditions, CDPs that led to racemic epoxychalcone **2** with the L,L series, led to racemic epoxychalcone **2** as expected (Table 2, entries 6, 8–10, 12–13, 17). However, CDPs that induced chirality in the asymmetric epoxydation of **1** were also effective catalysts, leading essentially to the same enantiomeric excesses, but with opposite chirality, providing (2*S*,3*R*)-epoxychalcone **2**.

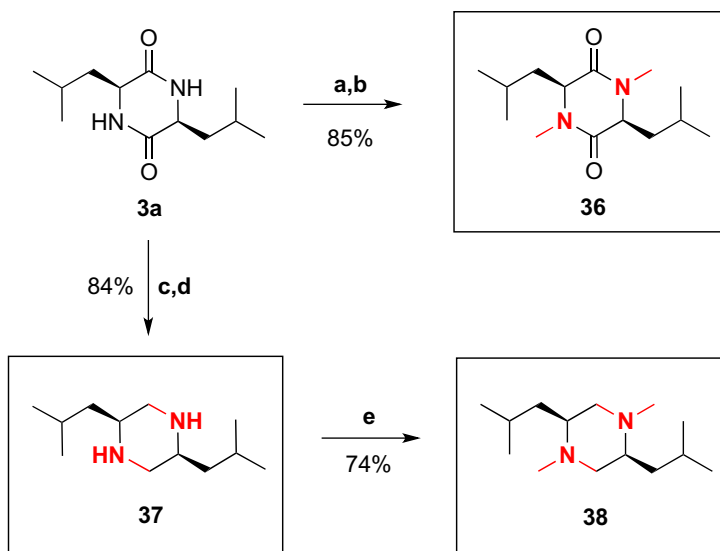
2.2.3. *trans*-(L,D) CDPs

We continued our investigation by evaluating the efficiency of *trans*-(L,D) CDPs in the asymmetric epoxidation of **1**. Thus, CDPs **3c**, **5c**, **10c**, **15c**, **19c**, **23c**, **26c**, and **31c** were prepared starting from the corresponding D and L-amino acids. Results of their efficacy are reported in Table 3. For CDPs **3c**, **19c**, **23c**, **26c**, and **31c**, having the same side chain substituents with opposite configuration led as expected to racemic epoxychalcone **2** due to their achiral structure (Table 3, entries 1, 5–8). CDP **5c**, which has an isobutyl and an isopropyl side chains facilitated the formation of (2*R*,3*S*)-epoxychalcone **2** with 5% ee, although with a very low 13% conversion (Table 3, entry 2). Interestingly, *trans* CDP **10c** provided (2*R*,3*S*)-**2** with 23% ee, the same enantiomer obtained with its *cis* analogue **10a**, albeit less efficiently (50% ee of (2*R*,3*S*)-**2**, Table 1, entry 3). This result demonstrates well that spatial orientation of side chains significantly impacts the stereochemical outcome of the process. CDP **15c** provided (2*R*,3*S*)-epoxychalcone **2** with 14% ee (Table 3, entry 4), an improvement as compared with its L,L analogue **15a** (Table 1, entry 13).

Overall, CDPs with isobutyl side chains led to higher enantioselectivities than those with one or two

Table 3. Catalytic efficiency of *trans*-(D,L) CDP in the triphasic epoxidation of *trans*-chalcone 1.

Entry	Supramolecular catalyst	Conversion (%)	ee (%)
1	<i>cyclo</i> [D-Leu-L-Leu] 3c	16	0
2	<i>cyclo</i> [D-Val-L-Leu] 5c	13	5 (2 <i>R</i> ,3 <i>S</i>)
3	<i>cyclo</i> [D-Pro-L-Leu] 5c	23	25 (2 <i>R</i> ,3 <i>S</i>)
4	<i>cyclo</i> [D-Ser(Bzl)-L-Phe] 15c	25	14 (2 <i>R</i> ,3 <i>S</i>)
5	<i>cyclo</i> [D-Phe-L-Phe] 19c	22	0
6	<i>cyclo</i> [D-Ala-L-Ala] 23c	24	0
7	<i>cyclo</i> [D-Ser(Bzl)-L-Ser(Bzl)] 26c	20	0
8	<i>cyclo</i> [D-Pro-L-Pro] 31c	15	0



a) NaH (3.0 equiv), DMF, 0 °C, 0.5 h. b) MeI (5.0 equiv), r.t., 3h. c) LiAlH₄ (12.0 equiv), THF, 0 °C to reflux, 48h d) Na₂SO₄•10 H₂O, 0 °C to reflux, 0.5 h. e) HCOOH (50 equiv), HCOH (33 equiv), 70 °C, 0.5h

Figure 6. (Colour online) Functional groups modification of CDP 3a.

aromatic side chains. This phenomenon, observed with leucine analogues, could be due to their ability to create more defined supramolecular catalytic superstructures at the interface. This is supported by the fact that their concave shape formed with *cis* substituents is essential for reactivity and introduction of chirality.

In addition, results with the tricyclic CDP 31a without any NH groups led to racemic epoxychalcone 2,

demonstrating the importance of the amide moiety to create supramolecular catalytic structures by hydrogen bonding. This is further supported by the results obtained with CDP 10a (with one secondary amide), which catalysed the formation of epoxide 2 with up to 50% ee. Substituting a leucine for a glycine in CDP leads to a significant drop in enantioselectivity.

Thus, it appears that two chiral side chains are essential to efficiently induce enantioselectivity.

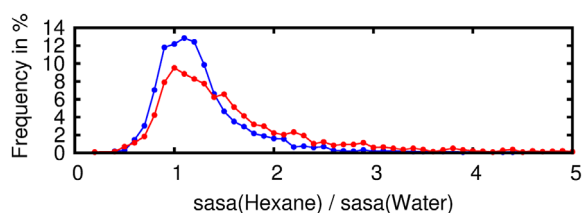


Figure 7. (Colour online) Frequency distributions of the SASA(hexane)/SASA(water) ratio for CDP **3a** (blue) and *trans*-chalcone **1** (red). Frequencies for each molecule sums to 100%. A ratio of one denotes an equal exposure to hexane and water.

2.2.4. CDP structure modifications

To further decipher the mechanism of the supramolecular process, we prepared structural analogues of the most efficient CDP **3a** (Figure 6) by modifying the NH and carbonyl groups. First, we used sodium hydride and methyl iodide to produce the *N*-methylated CDP **36**, with no hydrogen donor groups (19). We prepared the 14-piperazine **37** without hydrogen bond acceptor groups from **3a** with lithium aluminium hydride (LiAlH_4). Finally, we prepared *N,N*-dimethylpiperazine **38**, which lacks both hydrogen bond donors and acceptors (Figure 6) (20). Interestingly, using **36–38** in the process led to racemic epoxychalcone **2** with conversions near background reaction (<15%), confirming the results reported above and further supporting the necessity of amide moieties for the formation of efficient supramolecular catalytic complexes.

2.2.5. Mechanistic investigations using computational approaches

With the experimental results in hand and with the objective to elucidate the mechanism of this novel triphasic asymmetric epoxidation of acyclic enones, we performed thorough computational studies. First, the location and orientation of CDP **3a** and *trans*-chalcone **1** at the water/hexane interface were investigated using molecular

dynamic (MD) simulations. For this purpose, five 45-ns trajectories were recorded for each of CDP **3a** and *trans*-chalcone **1** in a water/hexane system. The results demonstrate that both molecules are located at the interface and adopt a limited range of conformations. Moreover, the two entities showed only 10% of non-specific contacts, suggesting that a sodium cation and/or a hydroperoxide anion are essential for the formation of a well-defined supramolecular complex.

To further characterise the location and orientation of both CDP **3a** and *trans*-chalcone **1** at the interface, we used the trajectories to calculate the solvent-accessible surface area (SASA) exposed by each molecule to each solvent. The ratio, SASA (hexane)/SASA(water), reveals the location respective to the interface. A ratio of 1 represents an interfacial positioning where the molecular surface is in equal contact with hexane and water, while a ratio higher than 1 indicates a greater exposure to hexane and a ratio lower than 1, a greater exposure to water. Figure 7 presents the frequency distribution of the SASA (hexane)/SASA (water) ratio for both molecules as calculated from the trajectories. The distributions show that both CDP **3a** and *trans*-chalcone **1** are located at the interface with a slightly higher exposure to hexane, in agreement with the predominance of non-polar functions present on each molecule. For CDP **3a**, the isobutyl side chains are in the hexane phase and the polar CDP ring is in the water phase (Figure 8). For *trans*-chalcone **1**, the preferred conformation is roughly planar at the interface with the carbonyl in the water phase. The interfacial location of CDP **3a** allows this molecule to position its hydrophilic functional groups, such as carbonyl and amide, in water while keeping the nonpolar functional groups, the isobutyl side chains, in contact with hexane (Figure 8).

Then, we measured the orientation of CDP **3a** and *trans*-chalcone **1** with respect to the interface obtained from the simulations. We used one vector (\vec{V}_1) for CDP **3a** and two vectors (\vec{V}_2 and \vec{V}_3) for *trans*-chalcone **1**. Figure 8

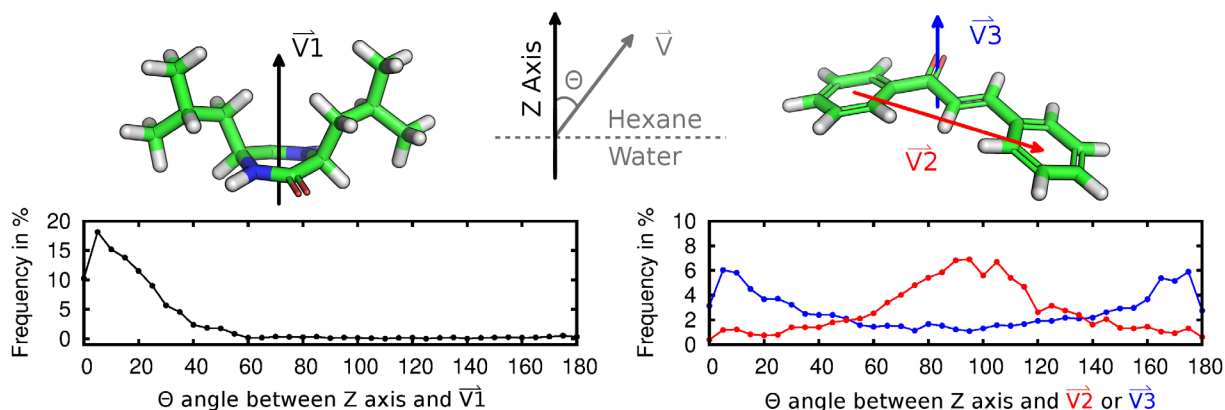


Figure 8. (Colour online) Orientation of CDP **3a** (left) and *trans*-chalcone **1** (right) with respect to the interface. Orientation is expressed as a distribution of angle θ between the Z axis (normal of the interface) and each vector \vec{V}_1 , \vec{V}_2 and \vec{V}_3 . Frequency for distribution profiles sums to 100%.

presents the angular deviation of these vectors from the normal of the interface (defined as Z axis). The $\overline{V1}$ vector presents an angular distribution between 0° and 40° with respect to the interfacial normal (Figure 8, left). This result suggests that the diketopiperazine ring of CDP **3a** lies almost parallel to the interface, as depicted in Figure 8 (top left). It also suggests that the fluctuations around this orientation are small, with the carbonyls going toward the water phase. The angular distributions of $\overline{V2}$ and $\overline{V3}$, presented in Figure 8 (right), indicate that the orientation of *trans*-chalcone **1** fluctuates more with respect to the interfacial normal. With a maximum distribution of $\sim 90^\circ$ for $\overline{V2}$, and $\sim 0^\circ$ for $\overline{V3}$, the most visited orientation of *trans*-chalcone **1** is almost parallel to the interface with its carbonyl pointing into the water phase.

2.2.5.1. Interfacial supramolecular assembly mediating enantioselective epoxidation. From experimental results, the CDP amide groups are essential for reactivity, both for their carbonyl (H-bond acceptor) or NH (H-bond donor). It is also reasonable to assume that the hydroperoxide anion tightly interacts with the sodium cation. From MD simulations, the CDP **3a** and *trans*-chalcone **1** do not interact together, suggesting that supramolecular complex formation is mediated by other species. On the basis of this information, we propose that the functional supramolecular complex involved in the catalysis consists of a bidentate system, in which the hydroperoxide anion and the sodium cation pair with the complementary donor and acceptor amide functions of the CDP. Then, *trans*-chalcone **1**, with its carbonyl group, interacts with the sodium cation. This latter interaction allows the molecule to position the reactive enone carbon close to the hydroperoxide (Figure 9).

To test this hypothesis, we built the following model. First, based on the results from the simulations, CDP **3a** and *trans*-chalcone **1** were placed on the same plane to

mimic the interfacial positioning. The sodium hydroperoxide anion was inserted in the middle at 2.3 \AA (21) between the sodium cation, the CDP **3a** carbonyl and the *trans*-chalcone **1** carbonyl. An arbitrary distance of 2.5 \AA and an angle of 107° were set to respect the Dunitz angle (22, 23) for nucleophilic attack between the hydroperoxide nucleophilic oxygen and the enone's reactive sp^2 carbon of *trans*-chalcone **1**. Figure 9 presents the proposed model for the functional supramolecular complex for CDP **3a** and *trans*-chalcone **1** resulting from energy minimisation. The geometry of the model is in agreement with a nucleophilic attack of the hydroperoxide anion on the chalcone enone. Furthermore, the proposed model is consistent with the orientation of hydrophilic and hydrophobic functional groups at the hexane/water interfacial position.

Because CDP **3a** is located at the interface with a small range of accessible orientations, the resulting supramolecular complex with a hydroperoxide anion and a sodium cation would retain its structure at the interface. Asymmetric epoxidation would occur upon efficient collision between this CDP **3a** complex and *trans*-chalcone **1**, also located at the interface with a planar orientation.

A reactive collision requires the *trans*-chalcone **1** carbonyl to interact with the sodium cation while having the enone reactive carbon on the same side as the hydroperoxide anion at a reactive distance as depicted in Figure 9 (left). Because of its unsymmetrical shape, *trans*-chalcone **1** can indiscriminately adopt two orientations at the interface. While one is reactive, the second is not, as shown in Figure 9 (right). With the latter orientation, the *trans*-chalcone **1** carbonyl interacts with the sodium cation, placing the enone's reactive carbon on the opposite side of the hydroperoxide anion, too far for reaction to occur. Consequently, only one enantiomer results from this supramolecular functional complex. The other enantiomer comes from the background reaction without the CDP intervention.

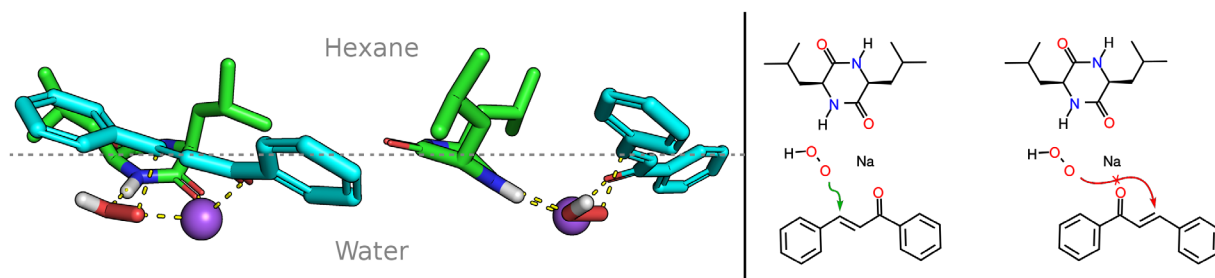


Figure 9. (Colour online) (Left) Optimised supramolecular complex proposed as model for the enantioselective epoxidation of **1** catalysed by CDP. CDP **3a** (green), *trans*-chalcone **1** (cyan), hydroperoxyde are in sticks and sodium is represented as a sphere. Only hydrogens involved in polar interactions are represented. The polar interactions are identified with dashed yellow lines. A grey dashed line is arbitrarily placed to represent the hexane/water interface. (Right) Illustration of the productive and non-productive supramolecular complexes.

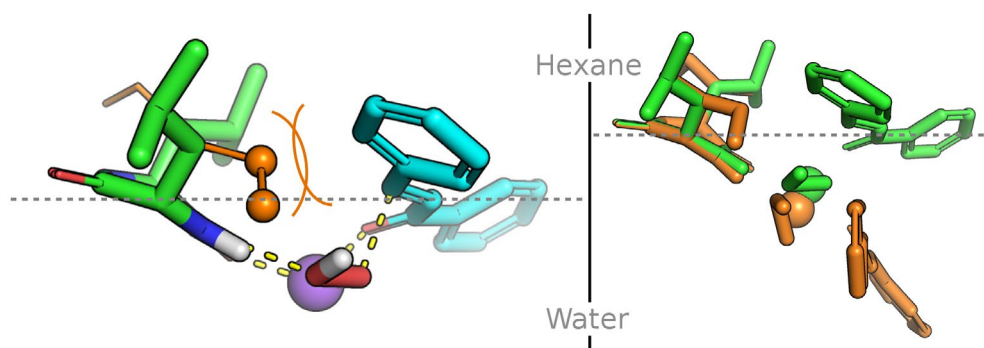


Figure 10. (Colour online) Comparison of the calculated models for functional supramolecular complex of CDP **3a** and CDP **25a**. (Left) CDP **3a** (green), CDP **25a** (orange), *trans*-chalcone **1** (cyan) and hydroperoxide are in sticks, sodium is a sphere. Only hydrogen involved in polar interactions are represented. The polar interactions are identified with dashed yellow lines. A grey dashed line is arbitrarily placed to represent the hexane/water interface. Clash between the ethyl chain on beta carbon of CDP **25a** (orange) with *trans*-chalcone **1** is shown with orange lines. (Right) Superimposition of the optimised supramolecular complex obtained with CDP **3a** in green and CDP **25a** in orange showing the two calculated position for **1**, the orange structure is located in water.

2.2.5.2. Impact of substitution at beta carbon. Figure 10 (left) presents the superimposition of *cyclo*[L-Ile-L-Ile], CDP **25a**, over the proposed functional supramolecular complex of CDP **3a**. According to the calculated structure, the ethyl chains on the beta carbon of CDP **25a** would clash with *trans*-chalcone **1**. The optimisation of the CDP **25a** supramolecular complex, as described in Section 2.2.5.1, resulted in a loose assembly. Figure 10 (right) shows a superimposition of the CDP **3a** (green) and CDP **25a** (orange) optimised supramolecular complexes. Considering the functional complex geometry proposed, for CDP **25a** to be positioned at the interface with the hydroperoxide anion and sodium cation in the water phase, the *trans*-chalcone **1** would be positioned completely in the water phase. This orientation is not favourable in a hexane/water system. Consequently, CDP **25a** is not functional and only a 15% yield of **2** is observed presumably originating from the background reaction without any enantioselectivity.

3. Conclusion

In summary, we have developed an efficient and rapid solid-phase synthesis using natural and synthetic amino acids to produce a library of CDPs. All of these CDPs were tested in the enantioselective epoxidation of enones in a two-phase system. Although most of the CDPs were not efficient in facilitating the process, some were effective catalysts for the epoxidation of *trans*-chalcone, leading to up to 70% ee in a triphasic system where the insoluble CDP resides at the water-hexane interface. The best CDP in our experiments was one derived from L-leucine. Our results revealed some structural features required for efficient conversion, and more importantly, to create a chiral

epoxide product. Depending on the side chain chirality of the CDPs, both enantiomers could be obtained. Our results showed that CDPs with their side chains in a *cis* relationship have higher reactivity. Reactivity was also influenced by the nature of the side chains. The level of enantioselectivity observed was highly variable, and seemed to rely on many parameters. Computational studies provided insights into the functional supramolecular interfacial complex that led to high enantioselectivity. The model we propose is consistent with the experimental data. On the basis of the reported results, we are working to improve the supramolecular catalytic efficiency of CDPs and to apply the concepts to various important organic reactions.

4. Experimental

4.1. General information

Oxime resin, coupling reagents and *N*-Boc-protected amino acids were purchased from Matrix Innovation (Québec City, QC, Canada). Resin with a substitution level of 1.12 mmol/g of oxime group was used. All chemicals were purchased from commercial sources and used directly, unless indicated otherwise. Nuclear magnetic resonance (NMR) spectra were recorded using Varian Inova 400 MHz and NMR Agilent DD2 500 MHz spectrometers. The coupling constants are reported in hertz (Hz). Chemical shifts are reported in parts per million downfield from TMS. Splitting patterns are designated as s (singlet), d (doublet), dd (doublet of doublets), t (triplet), q (quartet), brs (broad singlet), brt (broad triplet), brq (broad quadruplet) and m (multiplet). Mass spectra were obtained on an Agilent 6210 LC Time of Flight Mass Spectrometer in direct injection mode.

4.2. Preparation of CDPs (3-35)

4.2.1. Coupling of the first *N*-Boc protected α -amino acid on oxime resin

A desired quantity of oxime resin (1.12 mmol/g) was added to a peptide synthesis vessel. The resin was treated three times with CH_2Cl_2 . Amino acid (3.0 equiv) and HOBt (3.0 equiv) were dissolved in DMF in a 100-mL flask and the mixture was stirred for few minutes at 0 °C. DIC (3.0 equiv), DIEA (3.0 equiv) and DMAP (0.1 equiv) were added and the mixture was introduced into the peptide synthesis vessel and stirred mechanically for 3 h. The mixture was filtered under vacuum and the resin was washed (DMF (3 \times 100 mL), MeOH (3 \times 100 mL), DMF (3 \times 100 mL), MeOH (3 \times 100 mL)) and dried under reduced pressure.

4.2.2. Acetylation of unreacted sites on oxime resin

The resin was treated three times with DMF (3 \times 50 mL). A solution of 50% v/v DMF/acetic anhydride (80 mL) and DIEA (1 mL) were added to the peptide synthesis vessel and shaken for 1 h. Then, the mixture was filtered under vacuum and the resin was washed (DMF (3 \times 100 mL), MeOH (3 \times 100 mL), DMF (3 \times 100 mL), MeOH (3 \times 100 mL)) and dried under reduced pressure.

4.2.3. Removal of the *N*-Boc protecting group

The resin was treated three times with CH_2Cl_2 (100 mL). A 50% v/v solution of TFA in CH_2Cl_2 was added to the peptide synthesis vessel and shaken for 30 min. Then, the mixture was filtered under vacuum and the resin was washed with DMF (3 \times 100 mL), MeOH (3 \times 100 mL), DMF (3 \times 100 mL), MeOH (3 \times 100 mL) and with a solution of 10% v/v DIEA in CH_2Cl_2 (100 mL).

4.2.4. Coupling of the second *N*-Boc protected α -amino acid

The amino acid (3.0 equiv) was dissolved in DMF in a 100 mL flask. The solution was cooled to 0 °C, then HBTU (3.0 equiv) and HOBt (3.0 equiv) were added. The mixture was poured into the peptide synthesis vessel in which the resin has been previously treated with CH_2Cl_2 . DIEA (6.0 equiv) was also added to the vessel and the mixture was shaken for 3 h. After filtration under vacuum, the resin was washed (DMF (3 \times 100 mL), MeOH (3 \times 100 mL), DMF (3 \times 100 mL) and MeOH (3 \times 100 mL)) and dried under reduce pressure. The Kaiser ninhydrin test was performed to monitor the efficiency of the coupling, and the coupling procedure was repeated if needed.

4.2.5. Cyclisation/cleavage from the resin

First, *N*-Boc group was removed using procedure described in (Section 4.2.3), but without the 10% v/v DIEA/ CH_2Cl_2

washing step. After drying, CH_2Cl_2 and DIEA (2.5 equiv) were added to the peptide synthesis vessel and the mixture was shaken for 2 min. Acetic acid (5.0 equiv) was then added and the content was shaken for 24 h. Then the filtrate was collected and the resin was rinsed several times with CH_2Cl_2 and MeOH. All the filtrates were combined and evaporated, and the resulting solid was dissolved in CH_2Cl_2 . Amberlite IR-120 was introduced to the solution to remove remaining traces of DIEA. The mixture was stirred for a few minutes and filtered. The filtrate was evaporated to give compounds **3** to **35**. Trituration in a minimum of cold ether was performed and led to desired compounds with satisfying purity.

4.3. Spectral data of CDPs synthesised

4.3.1. (3*S*,6*S*)-3,6-diisobutylpiperazine-2,5-dione (**14**, **20**) (**3a**)

White powder. **¹H-NMR** (400 MHz, DMSO- d_6): δ = 0.81 (d, J = 6.5 Hz, 6H), 0.84 (d, J = 6.5 Hz, 6H), 1.35–1.45 (m, 2H), 1.49–1.57 (m, 2H), 1.70–1.81 (m, 2H), 3.64–3.69 (m, 2H), 8.14 (s, 2H). **¹³C-NMR** (101 MHz, DMSO- d_6): δ = 22.3, 23.7, 24.3, 44.3, 53.3, 169.2. **HRMS** (ESI-TOF, m/z): calcd for $\text{C}_{12}\text{H}_{23}\text{N}_2\text{O}_2$ ($M+H$)⁺ = 227.1754, found 227.1762.

4.3.2. (3*R*,6*R*)-3,6-diisobutylpiperazine-2,5-dione (**14**, **20**) (**3b**)

White powder. **¹H-NMR** (400 MHz, DMSO- d_6): δ = 0.81 (d, J = 6.5 Hz, 6H), 0.84 (d, J = 6.5 Hz, 6H), 1.35–1.45 (m, 2H), 1.49–1.57 (m, 2H), 1.70–1.81 (m, 2H), 3.64–3.69 (m, 2H), 8.14 (s, 2H). **¹³C-NMR** (101 MHz, DMSO- d_6): δ = 22.3, 23.7, 24.3, 44.3, 53.3, 169.2. **HRMS** (ESI-TOF, m/z): calcd for $\text{C}_{12}\text{H}_{23}\text{N}_2\text{O}_2$ ($M+H$)⁺ = 227.1754, found 227.1764.

4.3.3. (3*R*,6*S*)-3,6-diisobutylpiperazine-2,5-dione (**14**, **20**) (**3c**)

White powder. **¹H-NMR** (400 MHz, DMSO- d_6): δ = 0.81 (d, J = 6.3 Hz, 6H), 0.83 (d, J = 6.3 Hz, 6H), 1.40–1.59 (m, 4H), 1.69–1.83 (m, 2H), 3.67–3.74 (m, 2H), 8.08 (s, 2H). **¹³C-NMR** (101 MHz, DMSO- d_6): δ = 22.6, 23.5, 24.2, 42.0, 53.1, 169.4. **HRMS** (ESI-TOF, m/z): calcd for $\text{C}_{12}\text{H}_{23}\text{N}_2\text{O}_2$ ($M+H$)⁺ = 227.1754, found 227.1762.

4.3.4. (3*S*,6*S*)-3-isobutyl-6-methylpiperazine-2,5-dione (**24**) (**4a**)

White powder. **¹H-NMR** (400 MHz, DMSO- d_6): δ = 0.80 (d, J = 6.5 Hz, 3H), 0.83 (d, J = 6.5 Hz, 3H), 1.21 (d, J = 7.1 Hz, 3H), 1.37–1.45 (m, 1H), 1.52–1.60 (m, 1H), 1.71–1.74 (m, 1H), 3.68–3.75 (m, 1H), 3.78–3.85 (m, 1H), 8.06 (s, 1H), 8.08 (s, 1H). **¹³C-NMR** (101 MHz, DMSO- d_6): δ = 20.2, 22.5, 23.6, 24.3, 43.2, 50.5, 53.2, 169.0, 169.5. **HRMS** (ESI-TOF, m/z): calcd for $\text{C}_9\text{H}_{17}\text{N}_2\text{O}_2$ ($M+H$)⁺ = 185.1245, found 185.1301.

4.3.5. (3*R*,6*R*)-3-isobutyl-6-methylpiperazine-2,5-dione (4b)

White powder. **¹H-NMR** (400 MHz, DMSO-*d*₆): δ = 0.80 (d, *J* = 6.5 Hz, 3H), 0.83 (d, *J* = 6.5 Hz, 3H), 1.21 (d, *J* = 7.1 Hz, 3H), 1.37–1.45 (m, 1H), 1.52–1.60 (m, 1H), 1.71–1.74 (m, 1H), 3.68–3.75 (m, 1H), 3.78–3.85 (m, 1H), 8.06 (s, 1H), 808 (s, 1H). **¹³C-NMR** (101 MHz, DMSO-*d*₆): δ = 20.2, 22.5, 23.6, 24.3, 43.2, 50.5, 53.2, 169.0, 169.5. **HRMS** (ESI-TOF, *m/z*): calcd for C₉H₁₇N₂O₂ (M+H)⁺ = 185.1245, found 185.1292.

4.3.6. (3*S*,6*S*)-3-isobutyl-6-isopropylpiperazine-2,5-dione (24) (5a)

White powder. **¹H-NMR** (400 MHz, DMSO-*d*₆): δ = 0.79 (d, *J* = 3.0 Hz, 3H), 0.80 (d, *J* = 3.0 Hz, 3H), 0.83 (d, *J* = 6.8 Hz, 3H), 0.89 (d, *J* = 6.8 Hz, 3H), 1.34–1.43 (m, 1H), 1.52–1.62 (m, 1H), 1.79–1.85 (m, 1H), 2.05–2.12 (m, 1H), 3.55–3.59 (m, 1H), 3.68–3.74 (m, 1H), 8.01 (s, 1H), 8.14 (s, 1H). **¹³C-NMR** (101 MHz, DMSO-*d*₆): δ = 18.0, 19.4, 22.4, 23.8, 24.2, 32.1, 44.6, 53.0, 60.2, 167.5, 169.1. **HRMS** (ESI-TOF, *m/z*): calcd for C₁₁H₂₁N₂O₂ (M+H)⁺ = 213.1598, found 213.1608.

4.3.7. (3*R*,6*R*)-3-isobutyl-6-isopropylpiperazine-2,5-dione (20) (5b)

White powder. **¹H-NMR** (400 MHz, DMSO-*d*₆): δ = 0.79 (d, *J* = 3.0 Hz, 3H), 0.80 (d, *J* = 3.0 Hz, 3H), 0.83 (d, *J* = 6.8 Hz, 3H), 0.89 (d, *J* = 6.8 Hz, 3H), 1.34–1.43 (m, 1H), 1.52–1.62 (m, 1H), 1.79–1.85 (m, 1H), 2.05–2.12 (m, 1H), 3.55–3.59 (m, 1H), 3.68–3.74 (m, 1H), 8.01 (s, 1H), 8.14 (s, 1H). **¹³C-NMR** (101 MHz, DMSO-*d*₆): δ = 18.0, 19.4, 22.4, 23.8, 24.2, 32.1, 44.6, 53.0, 60.2, 167.5, 169.1. **HRMS** (ESI-TOF, *m/z*): calcd for C₁₁H₂₁N₂O₂ (M+H)⁺ = 213.1598, found 213.1601.

4.3.8. (3*R*,6*S*)-3-isobutyl-6-isopropylpiperazine-2,5-dione (5c)

White powder. **¹H-NMR** (400 MHz, DMSO-*d*₆): δ = 0.78–0.83 (m, 9H), 0.91 (d, *J* = 6.9 Hz, 3H), 1.44–1.59 (m, 2H), 1.71–1.84 (m, 1H), 2.10–2.20 (m, 1H), 3.60 (s, 1H), 3.67–3.74 (m, 1H), 7.96 (s, 1H), 8.08 (s, 1H). **¹³C-NMR** (101 MHz, DMSO-*d*₆): δ = 17.5, 19.0, 22.7, 23.5, 24.1, 31.9, 42.4, 53.0, 59.9, 168.1, 169.5. **HRMS** (ESI-TOF, *m/z*): calcd for C₁₁H₂₁N₂O₂ (M+H)⁺ = 213.1598, found 213.1607.

4.3.9. (3*S*,6*S*)-3-benzyl-6-isobutylpiperazine-2,5-dione (20) (6a)

White powder. **¹H-NMR** (400 MHz, DMSO-*d*₆): δ = 0.01–0.08 (m, 1H), 0.54 (d, *J* = 6.6 Hz, 3H), 0.80 (d, *J* = 6.6 Hz, 3H), 0.65–0.83 (m, 3H), 1.28–1.41 (m, 1H), 3.08 (dd, *J* = 13.6, 3.7 Hz, 1H), 3.38–3.45 (m, 1H), 4.09–4.15 (m, 1H), 7.05–7.25 (m, 5H), 8.02 (s, 1H), 8.04 (s, 1H). **¹³C-NMR** (101 MHz, DMSO-*d*₆): δ = 22.0, 23.5, 23.5, 39.1, 44.3, 52.9, 56.1, 127.4, 128.7, 131.1, 136.7, 166.8, 168.1. **HRMS** (ESI-TOF, *m/z*): calcd for C₁₅H₂₁N₂O₂ (M+H)⁺ = 261.1598, found 261.1608.

4.3.10. (3*R*,6*R*)-3-benzyl-6-isobutylpiperazine-2,5-dione (6b)

¹H-NMR (400 MHz, DMSO-*d*₆): δ = 0.01–0.08 (m, 1H), 0.54 (d, *J* = 6.6 Hz, 3H), 0.80 (d, *J* = 6.6 Hz, 3H), 0.65–0.83 (m, 3H), 1.28–1.41 (m, 1H), 3.08 (dd, *J* = 13.6, 3.7 Hz, 1H), 3.38–3.45 (m, 1H), 4.09–4.15 (m, 1H), 7.05–7.25 (m, 5H), 802 (s, 1H), 804 (s, 1H). **¹³C-NMR** (101 MHz, DMSO-*d*₆): δ = 22.0, 23.5, 23.5, 39.1, 44.3, 52.9, 56.1, 127.4, 128.7, 131.1, 136.7, 166.8, 168.1. **HRMS** (ESI-TOF, *m/z*): calcd for C₁₅H₂₁N₂O₂ (M+H)⁺ = 261.1598, found 261.1607.

4.3.11. (3*S*,6*S*)-3-isobutyl-6-(4-nitrobenzyl)piperazine-2,5-dione (7)

White powder. **¹H-NMR** (400 MHz, DMSO-*d*₆): δ = 0.16–0.25 (m, 1H), 0.48 (d, *J* = 6.5 Hz, 3H), 0.55 (d, *J* = 6.5 Hz, 3H), 0.76–0.84 (m, 1H), 1.29–1.39 (m, 1H), 2.95 (dd, *J* = 12.9, 5.1 Hz, 1H), 3.21 (dd, *J* = 13.4, 4.0 Hz, 1H), 3.46–3.52 (m, 1H), 4.22–4.26 (m, 1H), 7.37 (d, *J* = 8.4 Hz, 2H), 8.11–8.17 (m, 4H). **¹³C-NMR** (101 MHz, DMSO-*d*₆): δ = 22.1, 23.3, 23.5, 38.7, 44.3, 52.8, 55.7, 123.7, 132.3, 145.3, 147.3, 166.4, 168.1. **HRMS** (ESI-TOF, *m/z*): calcd for C₁₅H₂₀N₂O₄ (M+H)⁺ = 306.1448, found 306.1456.

4.3.12. (3*S*,6*S*)-3-(benzyloxymethyl)-6-isobutylpiperazine-2,5-dione (8a)

White powder. **¹H-NMR** (400 MHz, DMSO-*d*₆): δ = 0.64 (d, *J* = 6.5 Hz, 3H), 0.70 (d, *J* = 6.5 Hz, 3H), 1.37–1.51 (m, 2H), 1.62–1.72 (m, 1H), 3.49 (dd, *J* = 9.9, 2.7 Hz, 1H), 3.58–3.64 (m, 1H), 3.73 (dd, *J* = 9.4, 3.2 Hz, 2H), 3.86–3.89 (m, 1H), 4.42 (s, 2H), 7.21–7.30 (m, 5H), 8.04 (d, *J* = 2.5 Hz, 1H), 8.22 (d, *J* = 2.8 Hz, 1H). **¹³C-NMR** (101 MHz, DMSO-*d*₆): δ = 22.2, 23.6, 23.8, 45.0, 53.3, 56.1, 128.2, 128.3, 128.8, 138.6, 166.3, 168.8. **HRMS** (ESI-TOF, *m/z*): calcd for C₁₆H₂₃N₂O₃ (M+H)⁺ = 291.1703, found 291.1701.

4.3.13. (3*R*,6*R*)-3-(benzyloxymethyl)-6-isobutylpiperazine-2,5-dione (8b)

White powder. **¹H-NMR** (400 MHz, DMSO-*d*₆): δ = 0.64 (d, *J* = 6.5 Hz, 3H), 0.70 (d, *J* = 6.5 Hz, 3H), 1.37–1.51 (m, 2H), 1.62–1.72 (m, 1H), 3.49 (dd, *J* = 9.9, 2.7 Hz, 1H), 3.58–3.64 (m, 1H), 3.73 (dd, *J* = 9.4, 3.2 Hz, 2H), 3.86–3.89 (m, 1H), 4.42 (s, 2H), 7.21–7.30 (m, 5H), 8.04 (d, *J* = 2.5 Hz, 1H), 8.22 (d, *J* = 2.8 Hz, 1H). **¹³C-NMR** (101 MHz, DMSO-*d*₆): δ = 22.2, 23.6, 23.8, 45.0, 53.3, 56.1, 128.2, 128.3, 128.8, 138.6, 166.3, 168.8. **HRMS** (ESI-TOF, *m/z*): calcd for C₁₆H₂₃N₂O₃ (M+H)⁺ = 291.1703, found 291.1709.

4.3.14. (3*S*,6*S*)-3-(4-(benzyloxy)benzyl)-6-isobutylpiperazine-2,5-dione (20) (9a)

White powder. **¹H-NMR** (400 MHz, DMSO-*d*₆): δ = 0.08–0.15 (m, 1H), 0.58 (d, *J* = 6.7 Hz, 3H), 0.60 (d, *J* = 6.7 Hz, 3H), 0.70–0.77 (m, 1H), 1.32–1.45 (m, 1H), 2.71 (dd, *J* = 13.6, 4.9 Hz, 1H), 3.03 (dd, *J* = 13.6, 4.9 Hz, 2H), 3.38–3.42 (m, 1H),

4.04–4.08 (m, 1H), 4.97 (s, 2H), 6.87 (d, $J = 8.6$ Hz, 2H), 7.00 (d, $J = 8.6$ Hz, 2H), 7.23–7.38 (m, 5H), 8.04 (d, $J = 2.7$ Hz, 1H), 8.02 (d, $J = 2.2$ Hz, 1H). **$^{13}\text{C-NMR}$** (101 MHz, DMSO- d_6): $\delta = 21.8, 23.4, 23.6, 38.3, 52.9, 56.3, 69.9, 115.0, 128.3, 128.5, 128.8, 129.1, 132.0, 137.8, 158.2, 166.8, 168.1$. **HRMS** (ESI-TOF, m/z): calcd for $\text{C}_{22}\text{H}_{27}\text{N}_2\text{O}_3$ ($M+H$) $^+ = 367.2016$, found 367.2026.

4.3.15. (3*R*,6*R*)-3-(4-(benzyloxy)benzyl)-6-isobutylpiperazine-2,5-dione (20) (9b)

White powder. **$^1\text{H-NMR}$** (400 MHz, DMSO- d_6): $\delta = 0.08$ – 0.15 (m, 1H), 0.58 (d, $J = 6.7$ Hz, 3H), 0.60 (d, $J = 6.7$ Hz, 3H), 0.70–0.77 (m, 1H), 1.32–1.45 (m, 1H), 2.71 (dd, $J = 13.6, 4.9$ Hz, 1H), 3.03 (dd, $J = 13.6, 4.9$ Hz, 2H), 3.38–3.42 (m, 1H), 4.04–4.08 (m, 1H), 4.97 (s, 2H), 6.87 (d, $J = 8.6$ Hz, 2H), 7.00 (d, $J = 8.6$ Hz, 2H), 7.23–7.38 (m, 5H), 8.04 (d, $J = 2.7$ Hz, 1H), 8.02 (d, $J = 2.2$ Hz, 1H). **$^{13}\text{C-NMR}$** (101 MHz, DMSO- d_6): $\delta = 21.8, 23.4, 23.6, 38.3, 52.9, 56.3, 69.9, 115.0, 128.3, 128.5, 128.8, 129.1, 132.0, 137.8, 158.2, 166.8, 168.1$. **HRMS** (ESI-TOF, m/z): calcd for $\text{C}_{22}\text{H}_{27}\text{N}_2\text{O}_3$ ($M+H$) $^+ = 367.2016$, found 367.2022.

4.3.16. (3*S*,8*S*)-3-isobutylhexahydropyrrolo[12-*a*]pyrazine-14-dione (10a)

White powder. **$^1\text{H-NMR}$** (400 MHz, DMSO- d_6): $\delta = 0.82$ (dd, $J = 6.5, 3.5$ Hz, 6H), 1.24–1.36 (m, 1H), 1.65–1.92 (m, 5H), 2.01–2.12 (m, 1H), 3.24–3.37 (m, 3H), 3.95 (t, $J = 5.7$ Hz, 1H), 4.14 (t, $J = 8.0$ Hz, 1H), 7.97 (s, 1H). **$^{13}\text{C-NMR}$** (101 MHz, DMSO- d_6): $\delta = 22.3, 22.9, 23.2, 24.5, 27.8, 38.2, 45.3, 53.0, 58.9, 166.9, 170.8$. **HRMS** (ESI-TOF, m/z): calcd for $\text{C}_{11}\text{H}_{19}\text{N}_2\text{O}_2$ ($M+H$) $^+ = 211.1441$, found 211.1438.

4.3.17. (3*R*,8*S*)-3-isobutylhexahydropyrrolo[12-*a*]pyrazine-14-dione (25) (10c)

White powder. **$^1\text{H-NMR}$** (400 MHz, DMSO- d_6): $\delta = 0.87$ (d, $J = 6.3$ Hz, 3H), 0.91 (d, $J = 6.5$ Hz, 3H), 1.35–1.45 (m, 1H), 1.50–1.60 (m, 1H), 1.63–1.90 (m, 4H), 2.05–2.18 (m, 1H), 3.25–3.50 (m, 2H), 3.55–3.65 (m, 1H), 4.17 (dd, $J = 8.7, 6.8$ Hz, 1H), 8.35 (s, 1H). **$^{13}\text{C-NMR}$** (101 MHz, DMSO- d_6): $\delta = 21.5, 21.9, 23.0, 23.8, 28.5, 42.0, 44.8, 55.0, 57.5, 168.7$. **HRMS** (ESI-TOF, m/z): calcd for $\text{C}_{11}\text{H}_{19}\text{N}_2\text{O}_2$ ($M+H$) $^+ = 211.1441$, found 211.1438.

4.3.18. 3-(((2*S*,5*S*)-5-isobutyl-3,6-dioxopiperazin-2-yl)methyl)-1*H*-indole-1-carbaldehyde (11a)

White powder. **$^1\text{H-NMR}$** (400 MHz, DMSO- d_6): $\delta = 0.45$ (d, $J = 6.5$ Hz, 3H), 0.55 (d, $J = 6.5$ Hz, 3H), 0.87 (dd, $J = 14.5, 6.5$ Hz, 1H), 1.24 (dd, $J = 13.8, 7.0$ Hz, 1H), 3.03 (dd, $J = 14.4, 4.8$ Hz, 1H), 3.23 (dd, $J = 14.4, 3.5$ Hz, 1H), 3.51 (s, 1H), 4.21 (s, 1H), 7.33 (t, $J = 7.6$ Hz, 1H), 7.55 (s, 1H), 7.67 (d, $J = 7.8$ Hz, 1H), 8.10 (s, 1H), 8.16 (d, $J = 1.9$ Hz, 1H), 9.30 (s, 1H). **$^{13}\text{C-NMR}$** (101 MHz, DMSO- d_6): $\delta = 21.9, 23.1, 29.0, 44.3, 52.9, 55.2, 111.1, 115.5, 117.6, 120.5, 124.5, 125.1, 126.3,$

131.9, 161.8, 167.1, 167.9. **HRMS** (ESI-TOF, m/z): calcd for $\text{C}_{18}\text{H}_{22}\text{N}_3\text{O}_3$ ($M+H$) $^+ = 328.1656$, found 328.1659.

4.3.19. 1-(3-(((2*S*,5*S*)-5-isobutyl-3,6-dioxopiperazin-2-yl)propyl)-3-nitroguanidine (24) (12a)

White powder. **$^1\text{H-NMR}$** (400 MHz, DMSO- d_6): $\delta = 0.86$ (dd, $J = 12.6, 6.6$ Hz, 6H), 1.42–1.48 (m, 1H), 1.53–1.61 (m, 4H), 1.69–1.75 (m, 1H), 1.76–1.85 (m, 1H), 3.15 (brq, 2H), 3.72–3.77 (m, 2H), 8.15 (d, $J = 2.3$ Hz, 1H), 8.20 (d, $J = 2.3$ Hz, 1H), 8.56 (s, 1H), 9.42 (s, 1H), 11.14 (s, 1H). **$^{13}\text{C-NMR}$** (101 MHz, DMSO- d_6): $\delta = 22.2, 23.5, 24.1, 31.4, 40.7, 43.8, 53.0, 54.3, 159.8, 168.3, 168.8$. **HRMS** (ESI-TOF, m/z): calcd for $\text{C}_{12}\text{H}_{23}\text{N}_6\text{O}_4$ ($M+H$) $^+ = 315.1775$, found 315.1774.

4.3.20. (3*S*,6*S*)-3-benzyl-6-methylpiperazine-2,5-dione (26) (13a)

White powder. **$^1\text{H-NMR}$** (400 MHz, DMSO- d_6): $\delta = 0.40$ (d, $J = 6.9$ Hz, 3H), 2.80 (dd, $J = 13.7, 4.9$ Hz, 1H), 3.08 (dd, $J = 13.5, 5.6$ Hz, 1H), 3.53–3.60 (m, 1H), 4.15–4.10 (m, 1H), 7.07–7.15 (m, 2H), 7.14–7.26 (m, 3H), 7.97 (s, 1H), 8.07 (s, 1H). **$^{13}\text{C-NMR}$** (101 MHz, DMSO- d_6): $\delta = 20.4, 39.0, 50.4, 56.0, 127.3, 128.7, 131.0, 136.7, 166.5, 168.4$. **HRMS** (ESI-TOF, m/z): calcd for $\text{C}_{12}\text{H}_{15}\text{N}_2\text{O}_2$ ($M+H$) $^+ = 219.1128$, found 219.1139.

4.3.21. (3*R*,6*R*)-3-benzyl-6-methylpiperazine-2,5-dione (20) (13b)

White powder. **$^1\text{H-NMR}$** (400 MHz, DMSO- d_6): $\delta = 0.40$ (d, $J = 6.9$ Hz, 3H), 2.80 (dd, $J = 13.7, 4.9$ Hz, 1H), 3.08 (dd, $J = 13.5, 5.6$ Hz, 1H), 3.53–3.60 (m, 1H), 4.15–4.10 (m, 1H), 7.07–7.15 (m, 2H), 7.14–7.26 (m, 3H), 7.97 (s, 1H), 8.07 (s, 1H). **$^{13}\text{C-NMR}$** (101 MHz, DMSO- d_6): $\delta = 20.4, 39.0, 50.4, 56.0, 127.3, 128.7, 131.0, 136.7, 166.5, 168.4$. **HRMS** (ESI-TOF, m/z): calcd for $\text{C}_{12}\text{H}_{15}\text{N}_2\text{O}_2$ ($M+H$) $^+ = 219.1128$, found 219.1138.

4.3.22. (3*S*,6*S*)-3-benzyl-6-isopropylpiperazine-2,5-dione (26) (14a)

White powder. **$^1\text{H-NMR}$** (400 MHz, DMSO- d_6): $\delta = 0.19$ (d, $J = 7.0$ Hz, 3H), 0.59 (d, $J = 7.0$ Hz, 3H), 1.60–1.70 (m, 1H), 2.81 (dd, $J = 13.8, 4.7$ Hz, 1H), 3.10 (dd, $J = 13.8, 4.7$ Hz, 1H), 3.46–3.50 (m, 1H), 4.13–4.19 (m, 1H), 7.09–7.22 (m, 5H), 7.87 (s, 1H), 8.08 (s, 1H). **$^{13}\text{C-NMR}$** (101 MHz, DMSO- d_6): $\delta = 16.8, 18.9, 31.7, 38.4, 55.7, 59.8, 127.1, 128.6, 131.0, 137.0, 167.1, 167.2$. **HRMS** (ESI-TOF, m/z): calcd for $\text{C}_{14}\text{H}_{19}\text{N}_2\text{O}_2$ ($M+H$) $^+ = 247.1441$, found 247.1449.

4.3.23. (3*R*,6*R*)-3-benzyl-6-isopropylpiperazine-2,5-dione (14b)

White powder. **$^1\text{H-NMR}$** (400 MHz, DMSO- d_6): $\delta = 0.19$ (d, $J = 7.0$ Hz, 3H), 0.59 (d, $J = 7.0$ Hz, 3H), 1.60–1.70 (m, 1H), 2.81 (dd, $J = 13.8, 4.7$ Hz, 1H), 3.10 (dd, $J = 13.8$ et 4.7 Hz, 1H), 3.46–3.50 (m, 1H), 4.13–4.19 (m, 1H),

7.09–7.22 (m, 5H), 7.87 (s, 1H), 8.08 (s, 1H). **¹³C-NMR** (101 MHz, DMSO-*d*₆): δ = 16.8, 18.9, 31.7, 38.4, 55.7, 59.8, 127.1, 128.6, 131.0, 137.0, 167.1, 167.2. **HRMS** (ESI-TOF, *m/z*): calcd for C₁₄H₁₉N₂O₂ (M+H)⁺ = 247.1441, found 247.1459.

4.3.24. (3*S*,6*S*)-3-benzyl-6-(benzyloxymethyl)piperazine-2,5-dione (20) (15a)

White powder. **¹H-NMR** (400 MHz, DMSO-*d*₆): δ = 2.59 (dd, *J* = 9.7, 6.4 Hz, 1H), 2.86 (dd, *J* = 13.9, 50 Hz, 1H), 3.04 (dd, *J* = 13.5, 57 Hz, 1H), 3.23 (dd, *J* = 9.6, 3.0 Hz, 1H), 3.76–3.81 (m, 1H), 4.02–4.08 (m, 1H), 4.26 (s, 2H), 7.03 (d, *J* = 6.9 Hz, 2H), 7.13–7.32 (m, 8H), 8.07 (s, 2H). **¹³C-NMR** (101 MHz, DMSO-*d*₆): δ = 40.1, 55.6, 56.1, 72.2, 72.8, 127.2, 128.2, 128.3, 128.8, 128.9, 130.7, 137.1, 138.6, 165.7, 167.1. **HRMS** (ESI-TOF, *m/z*): calcd for C₁₉H₂₁N₂O₃ (M+H)⁺ = 325.1547, found 325.1555.

4.3.25. (3*R*,6*R*)-3-benzyl-6-(benzyloxymethyl)piperazine-2,5-dione (15b)

White powder. **¹H-NMR** (400 MHz, DMSO-*d*₆): δ = 2.59 (dd, *J* = 9.7, 6.4 Hz, 1H), 2.86 (dd, *J* = 13.9, 50 Hz, 1H), 3.04 (dd, *J* = 13.5, 57 Hz, 1H), 3.23 (dd, *J* = 9.6, 3.0 Hz, 1H), 3.76–3.81 (m, 1H), 4.02–4.08 (m, 1H), 4.26 (s, 2H), 7.03 (d, *J* = 6.9 Hz, 2H), 7.13–7.32 (m, 8H), 8.07 (s, 2H). **¹³C-NMR** (101 MHz, DMSO-*d*₆): δ = 40.1, 55.6, 56.1, 72.2, 72.8, 127.2, 128.2, 128.3, 128.8, 128.9, 130.7, 137.1, 138.6, 165.7, 167.1. **HRMS** (ESI-TOF, *m/z*): calcd for C₁₉H₂₁N₂O₃ (M+H)⁺ = 325.1547, found 325.1552.

4.3.26. (3*R*,6*S*)-3-benzyl-6-(benzyloxymethyl)piperazine-2,5-dione (15c)

White powder. **¹H-NMR** (400 MHz, DMSO-*d*₆): δ = 2.83 (dd, *J* = 13.8, 4.7 Hz, 1H), 3.10 (dd, *J* = 13.8, 4.7 Hz, 1H), 3.39 (dd, *J* = 9.6, 2.6 Hz, 1H), 3.63 (dd, *J* = 9.6, 2.6 Hz, 1H), 3.88–3.95 (m, 1H), 4.08–4.12 (m, 1H), 4.39 (dd, *J* = 4.4, 12.3 Hz, 1H), 7.12–7.31 (m, 10H), 7.98 (s, 1H), 8.16 (s, 1H). **¹³C-NMR** (101 MHz, DMSO-*d*₆): δ = 38.4, 55.5, 55.6, 71.4, 73.1, 127.3, 127.9, 128.7, 128.9, 130.5, 136.8, 138.8, 166.8, 166.9. **HRMS** (ESI-TOF, *m/z*): calcd for C₁₉H₂₁N₂O₃ (M+H)⁺ = 325.1547, found 325.1557.

4.3.27. Benzyl4-((2*S*,5*S*)-5-benzyl-3,6-dioxopiperazin-2-yl)butylcarbamate (16a)

White powder. **¹H-NMR** (500 MHz, DMSO-*d*₆): δ = 0.50–0.85 (m, 2H), 0.98–1.16 (m, 4H), 2.75–2.87 (m, 3H), 3.14 (dd, *J* = 13.4, 3.7 Hz, 1H), 3.36 (s, 1H), 3.55 (brs, 1H), 4.18 (brq, 1H), 5.00 (s, 2H), 7.11–7.26 (m, 6H), 7.28–7.39 (m, 4H), 8.02 (s, 1H), 8.14 (s, 1H). **¹³C-NMR** (126 MHz, DMSO-*d*₆): δ = δ 21.3, 29.4, 33.5, 38.6, 40.7, 54.2, 55.7, 65.6, 127.1, 128.2, 128.4, 128.8, 130.81, 136.5, 137.7, 156.4, 166.6, 167.4. **HRMS** (ESI-TOF, *m/z*): calcd for C₂₃H₂₈N₃O₄ (M+H)⁺ = 410.2074, found 410.2092.

4.3.28. (3*S*,6*S*)-3-(4-(benzyloxy)benzyl)-6-isopropylpiperazine-2,5-dione (17a)

White powder. **¹H-NMR** (400 MHz, DMSO-*d*₆): δ = 0.22 (d, *J* = 7.0 Hz, 3H), 0.60 (d, *J* = 7.0 Hz, 3H), 1.59–1.71 (m, 1H), 2.75 (dd, *J* = 14.0, 4.8 Hz, 1H), 3.03 (dd, *J* = 14.0, 48 Hz, 1H), 3.44–3.49 (m, 1H), 4.07–4.13 (m, 1H), 5.05 (s, 2H), 6.83 (d, *J* = 8.5 Hz, 2H), 7.03 (d, *J* = 8.5 Hz, 2H), 7.23–7.38 (m, 5H), 7.83 (s, 1H), 8.01 (s, 1H). **¹³C-NMR** (101 MHz, DMSO-*d*₆): δ = 16.8, 18.9, 31.7, 37.6, 55.8, 59.8, 69.7, 115.1, 128.1, 128.3, 129.0, 129.1, 131.9, 137.9, 157.9, 167.1, 167.3. **HRMS** (ESI-TOF, *m/z*): calcd for C₂₁H₂₅N₂O₃ (M+H)⁺ = 353.1860, found 353.1865.

4.3.29. (3*R*,6*R*)-3-(4-(benzyloxy)benzyl)-6-isopropylpiperazine-2,5-dione (17b)

White powder. **¹H-NMR** (400 MHz, DMSO-*d*₆): δ = 0.22 (d, *J* = 7.0 Hz, 3H), 0.60 (d, *J* = 7.0 Hz, 3H), 1.59–1.71 (m, 1H), 2.75 (dd, *J* = 14.0, 4.8 Hz, 1H), 3.03 (dd, *J* = 14.0, 48 Hz, 1H), 3.44–3.49 (m, 1H), 4.07–4.13 (m, 1H), 5.05 (s, 2H), 6.83 (d, *J* = 8.5 Hz, 2H), 7.03 (d, *J* = 8.5 Hz, 2H), 7.23–7.38 (m, 5H), 7.83 (s, 1H), 8.01 (s, 1H). **¹³C-NMR** (101 MHz, DMSO-*d*₆): δ = 16.8, 18.9, 31.7, 37.6, 55.8, 59.8, 69.7, 115.1, 128.1, 128.3, 129.0, 129.1, 131.9, 137.9, 157.9, 167.1, 167.3. **HRMS** (ESI-TOF, *m/z*): calcd for C₂₁H₂₅N₂O₃ (M+H)⁺ = 353.1860, found 353.1867.

4.3.30. 3-(((2*S*,5*S*)-5-benzyl-3,6-dioxopiperazin-2-yl)methyl)-1*H*-indole-1-carbaldehyde (18a)

White powder. **¹H-NMR** (400 MHz, DMSO-*d*₆): δ = 1.80 (dd, *J* = 13.5, 7.2 Hz, 1H), 2.41 (dd, *J* = 13.6, 4.7 Hz, 1H), 2.48 (dd, *J* = 12.8, 3.8 Hz, 1H), 2.76 (dd, *J* = 14.5, 4.1 Hz, 1H), 3.81 (brt, 1H), 3.93 (brt, 1H), 6.63–6.69 (m, 2H), 6.91–6.96 (m, 2H), 7.03 (t, *J* = 7.5 Hz, 1H), 7.08–7.17 (m, 3H), 7.28 (d, *J* = 8.0 Hz, 1H), 7.44 (d, *J* = 7.8 Hz, 1H), 7.67 (s, 1H), 7.87 (s, 1H), 10.85 (s, 1H). **¹³C-NMR** (101 MHz, DMSO-*d*₆): δ = 30.1, 55.7, 56.0, 109.2, 111.7, 118.8, 121.3, 124.8, 126.8, 128.4, 130.1, 136.4, 136.9, 166.6, 167.2. **HRMS** (ESI-TOF, *m/z*): calcd for C₂₁H₂₀N₃O₃ (M+H)⁺ = 362.4085, found 362.1505.

4.3.31. (3*S*,6*S*)-3,6-dibenzylpiperazine-2,5-dione (20) (19a)

White powder. **¹H-NMR** (400 MHz, DMSO-*d*₆): δ = 2.18 (dd, *J* = 14.1, 6.1 Hz, 2H), 2.52 (dd, *J* = 13.6, 4.9 Hz, 2H), 3.89–3.95 (m, 2H), 6.96–7.01 (m, 4H), 7.13–7.26 (m, 6H), 8.03 (s, 2H). **¹³C-NMR** (101 MHz, DMSO-*d*₆): δ = 40.0, 56.1, 127.2, 128.9, 130.5, 137.2, 166.8. **HRMS** (ESI-TOF, *m/z*): calcd for C₁₈H₁₉N₂O₂ (M+H)⁺ = 295.1441, found 295.1445.

4.3.32. (3*R*,6*R*)-3,6-dibenzylpiperazine-2,5-dione (20) (19b)

White powder. **¹H-NMR** (400 MHz, DMSO-*d*₆): δ = 2.18 (dd, *J* = 14.1, 6.1 Hz, 2H), 2.52 (dd, *J* = 13.6, 4.9 Hz, 2H), 3.89–3.95 (m, 2H), 6.96–7.01 (m, 4H), 7.13–7.26 (m, 6H), 8.03 (s,

2H). **¹³C-NMR** (101 MHz, DMSO-*d*₆): δ = 40.0, 56.1, 127.2, 128.9, 130.5, 137.2, 166.8. **HRMS** (ESI-TOF, *m/z*): calcd for C₁₈H₁₉N₂O₂ (M+H)⁺ = 295.1441, found 295.1450.

4.3.33. (3*R*,6*S*)-3,6-dibenzylpiperazine-2,5-dione (20) (19c)

White powder. **¹H-NMR** (400 MHz, DMSO-*d*₆): δ 2.67 (dd, *J* = 14.0, 8.0 Hz, 2H), 2.95 (dd, *J* = 12.0, 4.0 Hz, 2H), 3.33 (br, 2H), 7.06–7.09 (m, 4H), 7.16–7.22 (m, 6H), 8.01 (s, 2H). **¹³C-NMR** (101 MHz, DMSO-*d*₆): δ 32.2, 55.0, 127.0, 128.4, 130.1, 136.3, 167.3. **HRMS** (ESI-TOF, *m/z*): calcd for C₁₈H₁₉N₂O₂ (M+H)⁺ = 295.1441, found 295.1452.

4.3.34. (3*S*,6*S*)-3-benzyl-6-(4-nitrobenzyl)piperazine-2,5-dione (20a)

White powder. **¹H-NMR** (400 MHz, DMSO-*d*₆): δ = 2.16 (dd, *J* = 13.5, 6.5 Hz, 1H), 2.48 (dd, *J* = 13.5, 5.3 Hz, 1H), 2.66 (dd, *J* = 13.8, 5.1 Hz, 1H), 2.79 (dd, *J* = 13.6, 4.0 Hz, 1H), 3.95–4.01 (m, 1H), 4.07–4.12 (m, 1H), 7.02 (d, *J* = 7.4 Hz, 2H), 7.07–7.23 (m, 5H), 7.97–8.03 (m, 3H), 8.13 (s, 1H). **¹³C-NMR** (101 MHz, DMSO-*d*₆): δ = 38.8, 39.4, 55.5, 55.9, 123.8, 127.1, 128.7, 130.8, 131.5, 136.4, 145.7, 166.6, 166.7. **HRMS** (ESI-TOF, *m/z*): calcd for C₁₈H₁₈N₃O₄ (M+H)⁺ = 340.1292, found 340.1300.

4.3.35. (3*S*,6*S*)-3-benzyl-6-(4-(benzyloxy)benzyl)piperazine-2,5-dione (20) (21a)

White powder. **¹H-NMR** (400 MHz, DMSO-*d*₆): δ = 2.14 (dd, *J* = 13.8, 6.1 Hz, 1H), 2.22 (dd, *J* = 13.8, 6.1 Hz, 1H), 2.48–2.57 (m, 2H), 3.84–3.89 (m, 1H), 3.90–3.95 (m, 1H), 5.00 (s, 2H), 6.84–6.92 (m, 4H), 6.99 (d, *J* = 6.7 Hz, 2H), 7.12–7.35 (m, 8H), 7.84 (m, 2H). **¹³C-NMR** (101 MHz, DMSO-*d*₆): δ = 39.1, 42.4, 56.1, 56.2, 69.8, 115.2, 127.1, 128.1, 128.4, 128.9, 129.0, 129.3, 130.5, 131.5, 137.3, 137.8, 157.8, 166.9, 166.9. **HRMS** (ESI-TOF, *m/z*): calcd for C₂₅H₂₅N₂O₃ (M+H)⁺ = 401.1860, found 401.1865.

4.3.36. (3*R*,6*R*)-3-benzyl-6-(4-(benzyloxy)benzyl)piperazine-2,5-dione (21b)

White powder. **¹H-NMR** (400 MHz, DMSO-*d*₆): δ = 2.14 (dd, *J* = 13.8, 6.1 Hz, 1H), 2.22 (dd, *J* = 13.8, 6.1 Hz, 1H), 2.48–2.57 (m, 2H), 3.84–3.89 (m, 1H), 3.90–3.95 (m, 1H), 5.00 (s, 2H), 6.84–6.92 (m, 4H), 6.99 (d, *J* = 6.7 Hz, 2H), 7.12–7.35 (m, 8H), 7.84 (m, 2H). **¹³C-NMR** (101 MHz, DMSO-*d*₆): δ = 39.1, 42.4, 56.1, 56.2, 69.8, 115.2, 127.1, 128.1, 128.4, 128.9, 129.0, 129.3, 130.5, 131.5, 137.3, 137.8, 157.8, 166.9, 166.9. **HRMS** (ESI-TOF, *m/z*): calcd for C₂₅H₂₅N₂O₃ (M+H)⁺ = 401.1860, found 401.1869.

4.3.37. (3*S*,6*S*)-3-(4-(benzyloxy)benzyl)-6-(4-nitrobenzyl)piperazine-2,5-dione (22a)

White powder. **¹H-NMR** (500 MHz, DMSO-*d*₆): δ = 2.14 (dd, *J* = 13.6, 6.7 Hz, 1H), 2.20 (dd, *J* = 13.7, 6.1 Hz, 1H),

2.67 (dd, *J* = 13.7, 4.9 Hz, 1H), 2.76 (dd, *J* = 13.7, 4.4 Hz, 1H), 3.99 (t, *J* = 6.3 Hz, 1H), 4.08 (t, *J* = 4.4 Hz, 1H), 5.04 (s, 2H), 6.91–6.94 (m, 2H), 6.99–7.01 (m, 2H), 7.20 (d, *J* = 8.7 Hz, 2H), 7.25–7.30 (m, 3H), 7.35–7.37 (m, 2H), 8.00 (d, *J* = 2.2 Hz, 1H), 8.07–8.10 (m, 2H), 8.14 (d, *J* = 2.0 Hz, 1H). **¹³C-NMR** (125 MHz, DMSO-*d*₆): δ = 37.9, 40.1, 40.2, 55.3, 55.8, 69.5, 114.9, 123.6, 127.9, 128.1, 128.7, 128.8, 131.3, 131.6, 137.6, 145.7, 146.6, 157.7, 166.4, 166.8. **HRMS** (ESI-TOF, *m/z*): calcd for C₂₅H₂₄N₃O₅ (M+H)⁺ = 446.1710, found 446.1694

4.3.38. (3*S*,6*S*)-3,6-dimethylpiperazine-2,5-dione (23a)

White powder. **¹H-NMR** (400 MHz, DMSO-*d*₆): δ = 1.19 (d, *J* = 6.9 Hz, 6H), 3.79–3.89 (m, 2H), 8.04 (s, 2H). **¹³C-NMR** (101 MHz, DMSO-*d*₆): δ = 19.2, 50.4, 169.8. **HRMS** (ESI-TOF, *m/z*): calcd for C₆H₁₁N₂O₂ (M+H)⁺ = 143.0815, found 143.0822.

4.3.39. (3*R*,6*R*)-3,6-dimethylpiperazine-2,5-dione (23b)

White powder. **¹H-NMR** (400 MHz, DMSO-*d*₆): δ = 1.19 (d, *J* = 6.9 Hz, 6H), 3.79–3.89 (m, 2H), 8.04 (s, 2H). **¹³C-NMR** (101 MHz, DMSO-*d*₆): δ = 19.2, 50.4, 169.8. **HRMS** (ESI-TOF, *m/z*): calcd for C₆H₁₁N₂O₂ (M+H)⁺ = 143.0815, found 143.0819.

4.3.40. (3*S*,6*R*)-3,6-dimethylpiperazine-2,5-dione (28) (23c)

White powder. **¹H-NMR** (400 MHz, DMSO) : δ = 1.25 (d, *J* = 7.0 Hz, 6H), 3.83–3.90 (m, 2H), 8.10 (s, 2H). **¹³C-NMR** (400 MHz, DMSO): δ = 19.4, 50.3, 169.1. **HRMS** (ESI-TOF, *m/z*): calcd for C₆H₁₁N₂O₂ (M+H)⁺ = 143.0815, found 143.0818.

4.3.41. (3*S*,6*S*)-3,6-diisopropylpiperazine-2,5-dione (29) (24a)

White powder. **¹H-NMR** (400 MHz, DMSO-*d*₆): δ = 0.79 (d, *J* = 6.9 Hz, 6H), 0.91 (d, *J* = 6.9 Hz, 6H), 2.06–2.19 (m, 2H), 3.61–3.66 (m, 2H), 7.90 (s, 2H). **¹³C-NMR** (101 MHz, DMSO-*d*₆): δ = 17.9, 19.3, 31.7, 59.8, 168.1. **HRMS** (ESI-TOF, *m/z*): calcd for C₁₀H₁₉N₂O₂ (M+H)⁺ = 199.1441, found 199.1447 = (M+H)⁺

4.3.42. (3*R*,6*R*)-3,6-diisopropylpiperazine-2,5-dione (24b)

White powder. **¹H-NMR** (400 MHz, DMSO-*d*₆): δ = 0.79 (d, *J* = 6.9 Hz, 6H), 0.91 (d, *J* = 6.9 Hz, 6H), 2.06–2.19 (m, 2H), 3.61–3.66 (m, 2H), 7.90 (s, 2H). **¹³C-NMR** (101 MHz, DMSO-*d*₆): δ = 17.9, 19.3, 31.7, 59.8, 168.1. **HRMS** (ESI-TOF, *m/z*): calcd for C₁₀H₁₉N₂O₂ (M+H)⁺ = 199.1441, found 199.1451.

4.3.43. (3S,6S)-3,6-di-sec-butylpiperazine-2,5-dione (30) (25a)

White powder. **¹H-NMR** (400 MHz, DMSO): δ = 0.79 (t, J = 7.4 Hz, 6H), 0.89 (d, J = 7.1 Hz, 6H), 1.09–1.23 (m, 2H), 1.30–1.44 (m, 2H), 1.81–1.86 (m, 2H), 3.71 (t, J = 2.0 Hz, 2H), 7.88 (s, 2H). **¹³C-NMR** (400 MHz, DMSO): δ = 12.4, 15.4, 24.7, 38.1, 58.8, 167.9. **HRMS** (ESI-TOF, m/z): calcd for $C_{12}H_{23}N_2O_2$ (M+H)⁺ = 227.1754, found 227.1630.

4.3.44. (3S,6S)-3,6-bis(benzyloxymethyl)piperazine-2,5-dione (31) (26a)

White powder. **¹H-NMR** (400 MHz, DMSO- d_6): δ = 3.51 (dd, J = 9.7, 3.2 Hz, 2H), 3.62 (dd, J = 9.7, 3.2 Hz, 2H), 3.88–3.93 (m, 2H), 4.32 (s, 4H), 7.21–7.30 (m, 10H), 8.21 (s, 2H). **¹³C-NMR** (101 MHz, DMSO- d_6): δ = 55.9, 72.5, 72.9, 128.1, 128.2, 128.9, 138.6, 166.2. **HRMS** (ESI-TOF, m/z): calcd for $C_{20}H_{23}N_2O_4$ (M+H)⁺ = 355.1652, found 355.1662.

4.3.45. (3R,6R)-3,6-bis(benzyloxymethyl)piperazine-2,5-dione (26b)

White powder. **¹H-NMR** (400 MHz, DMSO- d_6): δ = 3.51 (dd, J = 9.7, 3.2 Hz, 2H), 3.62 (dd, J = 9.7, 3.2 Hz, 2H), 3.88–3.93 (m, 2H), 4.32 (s, 4H), 7.21–7.30 (m, 10H), 8.21 (s, 2H). **¹³C-NMR** (101 MHz, DMSO- d_6): δ = 55.9, 72.5, 72.9, 128.1, 128.2, 128.9, 138.6, 166.2. **HRMS** (ESI-TOF, m/z): calcd for $C_{20}H_{23}N_2O_4$ (M+H)⁺ = 355.1652, found 355.1659.

4.3.46. (3R,6S)-3,6-bis(benzyloxymethyl)piperazine-2,5-dione (31) (26c)

White powder. **¹H-NMR** (400 MHz, DMSO- d_6): δ = 3.54 (dd, J = 9.6, 2.3 Hz, 2H), 3.77 (dd, J = 9.6, 3.0 Hz, 2H), 3.89 (s, 2H), 4.45 (s, 4H), 7.22–7.34 (m, 10H), 8.16 (s, 2H). **¹³C-NMR** (400 MHz, DMSO): δ = 55.7, 71.1, 72.8, 127.7, 127.8, 128.7, 138.6, 167.0. **HRMS** (ESI-TOF, m/z): calcd for $C_{20}H_{23}N_2O_4$ (M+H)⁺ = 355.1652, found 355.1670.

4.3.47. (3S,6S)-3,6-bis((S)-1-(benzyloxy)ethyl)piperazine-2,5-dione (32) (27a)

White powder. **¹H-NMR** (400 MHz, DMSO): δ = 1.08 (d, J = 6.3 Hz, 6H), 3.57 (dd, J = 5.1, 3.6 Hz, 2H), 3.72–3.85 (m, 2H), 4.09 (d, J = 11.9 Hz, 2H), 4.26 (d, J = 11.9 Hz, 2H), 7.16–7.27 (m, 10H), 8.17 (s, 2H), 8.23 (s, 1H). **¹³C-NMR** (400 MHz, DMSO): δ = 16.7, 60.3, 70.4, 76.6, 127.7, 127.9, 128.5, 138.9, 166.4. **HRMS** (ESI-TOF, m/z): calcd for $C_6H_{11}N_2O_2$ (M+H)⁺ = 143.0815, found 143.0822.

4.3.48. (3S,6S)-3-(benzyloxymethyl)-6-isopropylpiperazine-2,5-dione (28a)

White powder. **¹H-NMR** (400 MHz, DMSO- d_6): δ = 0.78 (d, J = 6.9 Hz, 3H), 0.89 (d, J = 6.9 Hz, 3H), 2.08–2.17 (m, 1H), 3.53 (dd, J = 9.7, 2.8 Hz, 1H), 3.58–3.60 (m, 1H), 3.76 (dd, J = 9.7, 2.8 Hz, 1H), 3.89–3.92 (m, 1H), 4.45 (dd, J = 15.5, 9.3 Hz, 1H), 7.20–7.32 (m, 5H), 8.06 (s, 1H), 8.07 (s, 1H).

¹³C-NMR (101 MHz, DMSO- d_6): δ = 17.3, 18.9, 55.6, 60.1, 71.8, 73.1, 127.9, 128.1, 128.9, 138.8, 167.4, 168.3. **HRMS** (ESI-TOF, m/z): calcd for $C_{15}H_{21}N_2O_3$ (M+H)⁺ = 277.1547, found 277.1561.

4.3.49. (3R,6R)-3-(benzyloxymethyl)-6-isopropylpiperazine-2,5-dione (20) (28b)

White powder. **¹H-NMR** (400 MHz, DMSO- d_6): δ = 0.78 (d, J = 6.9 Hz, 3H), 0.89 (d, J = 6.9 Hz, 3H), 2.08–2.17 (m, 1H), 3.53 (dd, J = 9.7, 2.8 Hz, 1H), 3.58–3.60 (m, 1H), 3.76 (dd, J = 9.7, 2.8 Hz, 1H), 3.89–3.92 (m, 1H), 4.45 (dd, J = 15.5, 9.3 Hz, 1H), 7.20–7.32 (m, 5H), 8.06 (s, 1H), 8.07 (s, 1H). **¹³C-NMR** (101 MHz, DMSO- d_6): δ = 17.3, 18.9, 55.6, 60.1, 71.8, 73.1, 127.9, 128.1, 128.9, 138.8, 167.4, 168.3. **HRMS** (ESI-TOF, m/z): calcd for $C_{15}H_{21}N_2O_3$ (M+H)⁺ = 277.1547, found 277.1567.

4.3.50. (3S,6S)-3-(benzyloxymethyl)-6-sec-butylpiperazine-2,5-dione (29a)

White powder. **¹H-NMR** (400 MHz, DMSO- d_6): δ = 0.65 (t, J = 7.4 Hz, 3H), 0.82 (d, J = 7.1 Hz, 3H), 1.20 (q, J = 6.0 Hz, 2H), 1.73–1.85 (m, 1H), 3.05–3.12 (m, 2H), 3.55 (dd, J = 9.5, 2.9 Hz, 1H), 3.72 (dd, J = 9.6, 4.1 Hz, 1H), 4.33–4.51 (m, 2H), 7.17–7.33 (m, 5H), 8.05 (s, 1H), 8.08 (s, 1H). **¹³C-NMR** (101 MHz, DMSO- d_6): δ = 12.0, 15.5, 24.6, 38.7, 53.9, 59.3, 70.9, 72.9, 127.8, 127.9, 128.5, 138.5, 166.0, 167.0. **HRMS** (ESI-TOF, m/z): calcd for $C_{16}H_{23}N_2O_3$ (M+H)⁺ = 291.1703, found 291.1710.

4.3.51. 3-((2S,5S)-5-methyl-3,6-dioxopiperazin-2-yl)propanamide (33) (30a)

White powder. **¹H-NMR** (400 MHz, DMSO- d_6): δ = 1.25 (d, J = 7.0 Hz, 3H), 1.79–1.97 (m, 2H), 2.03–2.25 (m, 2H), 3.84–3.91 (m, 2H), 6.76 (s, 1H), 7.29 (s, 1H), 8.06 (s, 1H), 8.14 (s, 1H). **¹³C-NMR** (101 MHz, DMSO- d_6): δ = 19.6, 28.7, 30.7, 50.2, 54.0, 168.1, 169.4, 174.1. **HRMS** (ESI-TOF, m/z): calcd for $C_8H_{14}N_3O_3$ (M+H)⁺ = 200.1030, found 200.1025.

4.3.52. (3S,6S)-1,6-3,4-bis(propylidene)-1,4-piperazine-2,5-dione (34) (31a)

White powder. **¹H-NMR** (400 MHz, DMSO- d_6): δ = 1.86–1.95 (m, 2H), 1.97–2.07 (m, 2H), 2.12–2.23 (m, 2H), 2.26–2.35 (m, 4H), 3.46–3.56 (m, 2H), 4.13–4.19 (t, J = 7.9 Hz, 2H). **¹³C-NMR** (101 MHz, DMSO- d_6): δ = 23.6, 27.9, 45.4, 60.8, 166.6. **HRMS** (ESI-TOF, m/z): calcd for $C_{10}H_{15}N_2O_2$ (M+H)⁺ = 195.1128, found 195.1057.

4.3.53. (3R,6R)-1,6-3,4-bis(propylidene)-1,4-piperazine-2,5-dione (31b)

White powder. **¹H-NMR** (400 MHz, DMSO- d_6): δ = 1.86–1.95 (m, 2H), 1.97–2.07 (m, 2H), 2.12–2.23 (m, 2H), 2.26–2.35 (m, 4H), 3.46–3.56 (m, 2H), 4.13–4.19 (t, J = 7.9 Hz, 2H). **¹³C-NMR** (101 MHz, DMSO- d_6): δ = 23.6, 27.9, 45.4, 60.8, 166.6. **HRMS**

(ESI-TOF, m/z): calcd for $C_{10}H_{15}N_2O_2$ ($M+H$)⁺ = 195.1128, found 195.1054.

4.3.54. (3*S*,6*R*)-1,6-3,4-bis(propylidene)-1,4-piperazine-2,5-dione (31*c*)

White powder. ¹H-NMR (400 MHz, DMSO- d_6): δ = 1.70–1.84 (m, 2H), 1.85–1.99 (m, 2H), 1.99–2.01 (m, 2H), 2.40–2.49 (m, 2H), 3.28–3.37 (m, 2H), 3.95–4.03 (m, 4H). ¹³C-NMR (101 MHz, DMSO- d_6): δ = 23.5, 27.8, 45.4, 60.7, 166.6. HRMS (ESI-TOF, m/z): calcd for $C_{10}H_{15}N_2O_2$ ($M+H$)⁺ = 195.1128, found 195.1057.

4.3.55. (5*aR*,10*aR*)-tetrahydrodithiazolo[3,4-*a*:3',4'-*d'*]pyrazine-5,10(3*H*,8*H*)-dione (35) (32*a*)

White powder. ¹H-NMR (400 MHz, CDCl₃): δ = 4.76 (d, J = 10.0 Hz, 2H), 4.42–4.53 (m, 4H), 3.33–3.44 (m, 4H). ¹³C-NMR (101 MHz, CDCl₃): δ = 32.6, 48.5, 62.7, 163.7. HRMS (ESI-TOF, m/z): calcd for $C_8H_{11}N_2O_2S_2$ ($M+H$)⁺ = 231.0256, found 231.0256.

4.3.56. (5*S*)-3-isobutylpiperazine-2,5-dione (36) (33*a*)

White powder. ¹H-NMR (500 MHz, CDCl₃): δ = 0.86 (d, J = 6.6 Hz, 3H), 0.88 (d, J = 6.6 Hz, 3H), 1.49–1.56 (m, 2H), 1.70–1.80 (m, 1H), 3.58–3.70 (m, 2H), 3.80–3.84 (m, 1H), 7.96 (s, 1H), 8.22 (s, 1H). ¹³C-NMR (125 MHz, CDCl₃): δ = 21.6, 22.2, 23.3, 42.6, 44.7, 53.4, 166.7, 169.1. HRMS (ESI-TOF, m/z): calcd for $C_8H_{15}N_2O_2$ ($M+H$)⁺ = 171.1128, found 171.1133.

4.3.57. (5*S*)-3-benzylpiperazine-2,5-dione (26) (34*a*)

White powder. ¹H-NMR (400 MHz, DMSO- d_6): δ = 2.71 (d, J = 17.4 Hz, 1H), 2.83 (dd, J = 13.5, 4.0 Hz, 1H), 3.04 (dd, J = 13.5, 4.5 Hz, 1H), 3.32 (d, J = 2.8 Hz, 1H), 4.01 (brs, 1H), 7.11–7.13 (m, 2H), 7.17–7.26 (m, 3H). ¹³C-NMR (101 MHz, DMSO- d_6): δ = 39.2, 44.0, 55.9, 127.2, 128.5, 130.5, 136.4, 166.0, 167.5. HRMS (ESI-TOF, m/z): calcd for $C_{11}H_{13}N_2O_2$ ($M+H$)⁺ = 205.0972, found 205.0946.

4.3.58. (5*S*)-3-(benzyloxymethyl)piperazine-2,5-dione (37) (35*a*)

Orange powder ¹H-NMR (400 MHz, DMSO- d_6): δ = 3.48–3.86 (m, 5H), 4.45 (s, 2H), 7.20–7.33 (m, 5H), 8.03 (s, 1H), 8.13 (s, 1H). ¹³C-NMR (100 MHz, DMSO- d_6): δ = 41.5, 52.7, 69.2, 73.1, 127.8, 128.1, 128.9, 130.5, 138.8, 167.0, 167.2. HRMS (ESI-TOF, m/z): calcd for $C_{12}H_{15}N_2O_3$ ($M+H$)⁺ = 235.1077, found 235.1084.

4.4. Modification of CDP 3*a*

4.4.1. Preparation of (3*S*,6*S*)-3,6-diisobutyl-1,4-dimethylpiperazine-2,5-dione (19) (36)

At room temperature, **3a** was partially dissolved in DMF in an oven-dried three neck flask under argon.

The temperature was cooled down to 0 °C and NaH (3 equiv, 3 mmol). The mixture was stirred for 30 min and methyl iodide (5 equiv, 5 mmol) was added. The reaction mixture was allowed to warm at room temperature and stirred for 3 h. Water was added to the mixture and extracted three times with EtOAc. The organic layers were combined, washed with water and brine, dried with Na₂SO₄, concentrated *in vacuo* and purified by trituration using Et₂O yielding 254 mg (85%) of **8** as a pale yellow solid. ¹H-NMR (400 MHz, CDCl₃): δ = 0.94 (d, J = 6.6 Hz, 6H), 0.98 (d, J = 6.6 Hz, 6H), 1.51–1.58 (m, 2H), 1.64–1.71 (m, 2H), 1.83–1.98 (m, 2H), 2.93 (s, 6H), 3.79 (dd, J = 8.7, 5.0 Hz, 2H). ¹³C-NMR (100 MHz, CDCl₃): δ = 22.0, 23.0, 25.2, 32.7, 43.7, 60.8, 166.8. HRMS (ESI-TOF, m/z): calcd for $C_{14}H_{27}N_2O_2$ ($M+H$)⁺ = 255.2067, found 255.2071.

4.4.2. Preparation of (2*S*,5*S*)-2,5-diisobutylpiperazine (20) (37)

The CDP **3a** was partially dissolved in anhydrous THF in an oven-dried three-neck flask under argon. The solution was cooled to 0 °C and LiAlH₄ (1.0 M THF, 12 eq) was added dropwise. The mixture was allowed to warm at room temperature and the reaction was refluxed overnight. The mixture was then cooled to 0 °C and treated with Na₂SO₄ decahydrate. The suspension obtained was refluxed for 30 min and then filtered. The solvent was evaporated under reduced pressure and the crude product was dried under vacuum yielding **9** as a pale oil (66% yield). (2*S*,5*S*)-2,5-diisobutylpiperazine (**37**); ¹H-NMR (400 MHz, DMSO- d_6): δ 0.80 (d, J = 6.4 Hz, 12H), 1.21–1.41 (m, 4H), 1.53–1.62 (m, 2H), 2.52 (dd, J = 12.1, 5.7 Hz, 2H), 2.74–2.82 (m, 4H), 7.76 (s, 2H). ¹³C-NMR (101 MHz, DMSO) δ 22.9, 23.1, 24.2, 45.2, 50.0. HRMS (ESI-TOF, m/z): calcd for $C_{12}H_{27}N_2$ ($M+H$)⁺ = 199.2129, found 199.2258.

4.4.3. Preparation of (2*S*,5*S*)-2,5-diisobutyl-1,4-dimethylpiperazine (20) (38)

Without purification, the 14-piperazine **37** from previous step was dissolved in formic acid (50 eq) in a regular round bottom flask and stirred for a few minutes. Formaldehyde (33 eq, 37% v/v in water) was added and the mixture was stirred at 70 °C for 30 min. EtOAc was used to dilute the reaction mixture and a saturated NaHCO₃ solution was added dropwise until no further gas formation was observed. The reaction mixture was extracted three times with EtOAc. The organic layers were combined, dried with Na₂SO₄, filtered, concentrated *in vacuo* and purified by flash chromatography using (90:5:5) CH₂Cl₂/MeOH/AcOH yielding **10** as a red oil (17% yield). ¹H-NMR (400 MHz, CDCl₃): δ = 0.87 (d, J = 6.6 Hz, 3H), 0.91 (d, J = 6.6 Hz, 3H), 1.31–1.41 (m, 4H), 1.49–1.61 (m, 2H), 2.27 (s, 6H), 2.29–2.50 (m, 6H). ¹³C-NMR (100 MHz, CDCl₃): δ = 22.2, 24.2, 26.0, 36.2, 42.8, 56.8, 59.2.

HRMS (ESI-TOF, m/z) calcd for $C_{14}H_{31}N_2$ (M+H)⁺ = 227.2482, found 227.2490.

4.5. Typical procedure for the asymmetric epoxidation of trans-chalcone 1

The catalyst (0.01 mmol, 0.1 equiv.) was added to a solution of enone (0.1 mmol) in 0.3 mL of hexanes and stirred at room temperature for 30 min. Then, 0.2 mL of a solution of 25% NaOH (m/v) in 30% H₂O₂ (w/w) was added and the mixture was stirred in the dark at room temperature for 48 h. 25 μ L of H₂O₂ 30% were added to the solution after 24 h. The conversion and the enantiomeric excess of the corresponding epoxychalcone were determined by chiral HPLC using a Hewlett Packard series 1050 using the following conditions: *trans*-(2*R*,3*S*)-Epoxy-1,3-diphenylpropan-1-one (**2**). HPLC (Chiralcel OD-H): λ 254 nm, hexanes/*i*-PrOH 95/5, flow rate 0.6 mL/min, t_r (2*S*,3*R*) = 19.23 min, t_r (2*R*,3*S*) = 21.29 min (14, 38). Each epoxidation reaction has been done at least in duplicate and the reported results correspond to the means of the experiments (conversions and enantiomeric excesses).

4.6. MD simulations

4.6.1. Trans-chalcone 1 parametrisation

Trans-chalcone **1** molecule was built in MOE (www.chem-comp.com). Initial parameters for the CHARMM general force field (CGenFF v 3.0.1) (39, 40), were automatically assigned using the CGenFF paramchem server (cgenff.paramchem.org) (41, 42). Parameters for charges, angles and dihedral angles with penalties above 10 were optimised using the Force Field Toolkit (FFTK) (43) implemented in VMD 1.9.2. (44) Figure S1 shows the optimised parameters on the *trans*-chalcone **1** molecule. Target quantum mechanical (QM) data were computed with Gaussian 03 (45) using the input files generated through the FFTK workflow using default parameters. Charges were optimised using default FFTK procedure until convergence. The first round of optimisation for the angle used an angle deviation of 2.0°, a constant K Upper Bound of 60 kcal/mol with the simulated annealing protocol. The obtained bond constant was further optimised until convergence using an angle deviation of 0 and the downhill algorithm. First round of dihedral angles optimisation used a k_{\max} of 3 with the simulated annealing protocol and default parameters. The obtained dihedral angle constants were further refined with the downhill protocol until convergence to a RMSE of 0.105°. Figure S2 presents the target potential energy surface from QM used for dihedral angles parametrisation, the PSE using missing parameters with $k = 0$ and the PSE with optimised dihedral angles parameters.

The topology and parameters for the *trans*-chalcone **1** are provided as supplementary material.

4.6.2. System preparation

CDP **3a** was built in MOE and prepared for MD simulations using the charmm-gui web server (46) Two orthogonal boxes of dimension $x = y = 40$ Å and $z = 30$ Å, one composed of water and the other of hexane, were joined together using packmol version 15084 (47) yielding a system of dimension $x = y = 40$ Å and $z = 60$ Å CDP **3a** and *trans*-chalcone **1** were initially positioned in the water and hexane phases, respectively, with their respective geometric centre at 105 Å of the interface and at 21 Å of each other Na⁺ and Cl⁻ were added to the water phase at a concentration of 0.15 M and neutral net charge.

4.6.3. Simulations

All the MD simulations were performed using NAMD 2.9 (48) using the CHARMM36 force field (49), TIP3 waters (50, 51), periodic boundary conditions and a timestep of 2 fs for long-range electrostatics and 1 fs for all other potentials. Cut-offs for the short-range electrostatics and the Lennard-Jones interactions were 12 Å with the latter smoothed via a switching function over the range of 10 to 12 Å. Long-range electrostatics were calculated via the Particle Mesh Ewald method (52, 53) using a sixth-order interpolation and a grid spacing of ≈ 1 Å NPT ensembles were generated Langevin damping with a coefficient of 1 ps⁻¹ was used to maintain a constant temperature of 37 °C, and the pressure was controlled by a Nosé-Hoover Langevin piston at 1 atm. The length of the bonds between hydrogens and heavy atoms were constrained using the SETTLE (54) for water molecules, and SHAKE (55) for all other molecules The x - y plane area was kept constant allowing fluctuation of the z axis Nonbonded pair lists were updated every 10 steps The systems were minimised for 300 steps prior to MD simulations. Five 45 ns trajectories were recorded, for a total of 225 ns of trajectories, and the coordinates were saved every 100 ps for analysis with the first 3 ns of each trajectory considered as equilibration.

4.6.4. Analysis

Solvent accessible surface area (SASA) was calculated for CDP **3a** and *trans*-chalcone **1** using the measure function in VMD with a radius (srad) of 14 Å. The distributions of orientations adopted by the molecules relative to the normal of the interface (Z axis) were calculated using one vector for the CDP **3a** ($\vec{V1}$) and two vectors the *trans*-chalcone **1** ($\vec{V2}$ and $\vec{V3}$) (see Figure 8). For CDP **3a**, $\vec{V1}$ was defined as the cross product of the vector between the two amide nitrogens and the vector between the two carbonyl oxygens. The first vector of *trans*-chalcone **1** ($\vec{V2}$) was defined as

by the geometric centres of the two benzene rings, while $\overline{V3}$ was defined as the cross product of $\overline{V2}$ and the vector described by the bond between the carbonyl carbon and oxygen (Figure 8).

4.7. Establishment of the functional supramolecular complex model

All molecules were initially built and individually optimised in MOE using default parameters. The supramolecular complex was composed of CDP **3a**, *trans*-chalcone **1**, sodium cation and hydroperoxide anion. Based on the interfacial positioning of the molecules observed from MD simulations, CDP **3a** and *trans*-chalcone **1** were started on the same plane. Sodium cation and hydroperoxide anion were placed in between the molecules, with a separation distance of 2.3 Å (21) between the sodium cation and the CDP **3a** carbonyl, the *trans*-chalcone **1** carbonyl and the hydroperoxide anion. In addition, the hydroperoxide was positioned at a distance of 2.5 Å (arbitrary) and an angle of 107° between the hydroperoxide anionic oxygen and the enone reactive carbon of *trans*-chalcone **1**, according to the dunitz angle for nucleophilic attack (22, 23). This initial positioning was then optimised using density functional theory (DFT) calculations at the B97-D3 (56)/Def2-SVP (57) level. The resulting complex was further optimised without constraint at the B97-D3 (56) / Def2-TZVP (57) level. The above procedure was also used to build the supramolecular complex with CDP **25a**. Finally, a relaxed scan of the distance between hydroperoxide anionic oxygen and the enone reactive carbon of *trans*-chalcone **1** (from 2.3 to 1.3 Å), was realised for the supramolecular CDP **3a** complex. This scan confirmed the reactivity of this complex and the absence of transition state on the potential energy surface for this supramolecular complex. All QM calculations were performed using Orca 3.0.3 software (58) and used the empirical D3 correction (59, 60), (denoted by the suffix -D3), and the Becke-Johnson damping potential (61), and the RIJCOSX approximation (62), as recommended (63).

Acknowledgements

The authors thank François Otis for his technical assistance with liquid chromatography and in peptide synthesis. This work was supported by the NSERC of Canada, the FQRNT of Quebec, PROTEO and Université Laval. C.B. is also indebted to FRQNT for a postgraduate scholarship.

Disclosure statement

No potential conflict of interest was reported by the authors.

Funding

This work was supported by the NSERC of Canada, the FQRNT of Quebec, PROTEO and Université Laval.

References

- (1) Raj, M.; Singh, V.K. *Chem. Commun.* **2009**, 44, 6687–6703.
- (2) Gruttadauria, M.; Giacalone, F.; Noto, R. *Adv. Synth. Catal.* **2009**, 351, 33–57.
- (3) Jimeno, C. *Org. Biomol. Chem.* **2016**, 14, 6147–6164.
- (4) Hernández, J.G.; Juaristi, E. *Chem. Commun.* **2012**, 48, 5396–5409.
- (5) Raynal, M.; Ballester, P.; Vidal-Ferran, A.; van Leeuwen, P.W.N.M. *Chem. Soc. Rev.* **2014**, 43, 1734–1787.
- (6) Oku, J.-I.; Inoue, S. *J. Chem. Soc. Chem. Commun.* **1981**, 229–230.
- (7) Iyer, M.S.; Gigstad, K.; Namdev, N.; Lipton, M. *J. Am. Chem. Soc.* **1996**, 118, 4910–4911.
- (8) Kogut, E.F.; Thoen, J.C.; Lipton, M.A. *J. Org. Chem.* **1998**, 63, 4604–4610.
- (9) Wang, Z.Y.; Shen, J.; Jaing, C.S.; You, C.P. *Chin. Chem. Lett.* **2000**, 11, 659–662.
- (10) Furutani, M.; Sakamoto, S.; Kudo, K. *Heterocycles* **2009**, 78, 1171–1176.
- (11) Durini, M.; Sahr, F.A.; Kuhn, M.; Civera, M.; Gennari, C.; Piarulli, U. *Eur. J. Org. Chem.* **2011**, 28, 5599–5607.
- (12) Ressurreição, A.S.M.; Delatouche, R.; Gennari, C.; Piarulli, U. *Eur. J. Org. Chem.* **2011**, 2, 217–228.
- (13) Borthwick, A. *Chem. Rev.* **2012**, 112, 3641–3716.
- (14) Bérubé, C.; Voyer, N. *Synth. Commun.* **2016**, 46, 395–403.
- (15) Berkessel, A.; Gasch, N.; Glaubitz, K.; Koch, C. *Org. Lett.* **2001**, 3, 3839–3842.
- (16) DeGrado, W.F.; Kaiser, E.T. *J. Org. Chem.* **1980**, 45, 1295–1300.
- (17) DeGrado, W.F.; Kaiser, E.T. *J. Org. Chem.* **1982**, 47, 3258–3261.
- (18) Smith, R.A.; Bobko, M.A.; Lee, W. *Bioorg. Med. Chem. Lett.* **1998**, 8, 2369–2374.
- (19) Durow, A.; Long, G.; O'Connell, S.J.; Willis, C. *Org. Lett.* **2006**, 8, 5401–5404.
- (20) Bérubé, C.; Cardinal, S.; Boudreault, P.L.; Barbeau, X.; Delcey, N.; Giguère, M.; Gleeton, D.; Voyer, N. *Tetrahedron* **2015**, 71, 8077–8084.
- (21) Rao, J.S.; Dinadayalane, T.C.; Leszczynski, J.; Sastry, G.N. *J. Phys. Chem. A* **2008**, 112, 12944–12953.
- (22) Bürgi, H.B.; Dunitz, J.D.; Lehn, J.M.; Wipff, G. *Tetrahedron* **1974**, 30, 1563–1572.
- (23) Cieplak, A.S. Organic Addition and Elimination Reactions; Transformation Paths of Carbonyl Derivatives. In *Structure Correlation*; Bürgi, Hans-Beat, Dunitz, Jack D., Eds.; Wiley-VCH Verlag GmbH: Weinheim, Germany, **1994**, Vol. 1, pp 205–302. Chapter 6.
- (24) Furukawa, T.; Akutagawa, T.; Funatani, H.; Uchida, T.; Hotta, Y.; Niwa, M.; Takaya, Y. *Bioorg. Med. Chem.* **2012**, 20, 2002–2009.
- (25) Monbaliu, J.C.M.; Hansen, F.K.; Beagle, L.K.; Panzner, M.J.; Steel, P.J.; Todadze, E.; Stevens, C.V.; Katritzky, A.R. *Chem. Eur. J.* **2012**, 18, 2632–2638.
- (26) Nakao, M.; Toriuchi, Y.; Fukayama, S.; Sano, S. *Chem. Lett.* **2014**, 43, 340–342.

- (27) Tanatani, A.; Mio, M.J.; Moore, J.S. *J. Am. Chem. Soc.* **2001**, *123*, 1792–1793.
- (28) Kricheldorf, H.R. *Org. Magn. Reson.* **1980**, *13*, 52–58.
- (29) Tanihara, M.; Hiza, T.; Imanishi, Y.; Higashimura, T. *Bull. Chem. Soc. Jpn.* **1983**, *56*, 1155–1160.
- (30) Cook, B.; Hill, R.R.; Jeffs, G.E. *J. Chem. Soc. Perkin Trans.* **1992**, *1*, 1199–1201.
- (31) Witiak, D.T.; Nair, R.V.; Schmid, F.A. *J. Med. Chem.* **1985**, *28*, 1228–1234.
- (32) Li, S.-Q.; Yang, Y.-B.; Yang, X.-Q.; Jiang, Y.; Li, Z.-J.; Li, X.-Z.; Chen, X.; Li, Q.-L.; Qin, S.-H.; Ding, Z.-T. *Helv. Chim. Acta* **2016**, *99*, 210–214.
- (33) Sano, T.; Sugaya, T.; Inoue, K.; Mizutaki, S.-I.; Ono, Y.; Kasai, M. *Org. Proc. Res. Dev.* **2000**, *4*, 147–152.
- (34) Stark, T.; Hofmann, T. *J. Agric. Food Chem.* **2005**, *53*, 7222–7231.
- (35) González, A.; Vorobeva, S.L.; Linares, A. *Tetrahedron: Asymmetry* **1995**, *6*, 1357–1366.
- (36) Beagle, L.; Hansen, F.; Monbaliu, J.; Desrosiers, M.P.; Phillips, A.; Stevens, C.; Katritzky, A. *Synlett* **2012**, *23*(16), 2337–2340.
- (37) Ashton, K.S.; Denti, M.; Norman, M.H.; St. Jean, D.J. *Tetrahedron. Lett.* **2014**, *55*, 4501–4504.
- (38) Lu, J.; Xu, Y.-H.; Liu, F.; Loh, T.-P. *Tetrahedron. Lett.* **2008**, *49*, 6007–6008.
- (39) Vanommeslaeghe, K.; Hatcher, E.; Acharya, C.; Kundu, S.; Zhong, S.; Shim, J.; Darian, E.; Guvench, O.; Lopes, P.; Vorobyov, I.; Mackerell, A.D. *J. Comput. Chem.* **2010**, *31*, 671–690.
- (40) Yu, W.; He, X.; Vanommeslaeghe, K.; MacKerell, A.D. *J. Comput. Chem.* **2012**, *33*, 2451–2468.
- (41) Vanommeslaeghe, K.; MacKerell, A.D. *J. Chem. Inf. Model.* **2012**, *52*, 3144–3154.
- (42) Vanommeslaeghe, K.; Raman, E.P.; MacKerell, A.D. *J. Chem. Inf. Model.* **2012**, *52*, 3155–3168.
- (43) Mayne, C.G.; Saam, J.; Schulten, K.; Tajkhorshid, E.; Gumbart, J.C. *J. Comput. Chem.* **2013**, *34*, 2757–2770.
- (44) Humphrey, W.; Dalke, A.; Schulten, K. *J. Mol. Graphics* **1996**, *14*, 33–38.
- (45) Frisch, M.J.; Trucks, G.W.; Schlegel, H.B.; Scuseria, G.E.; Robb, M.A.; Cheeseman, J.R.; Montgomery, J.A.; Vreven, T.; Kudin, K.N.; Burant, J.C.; Millam, J.M.; Iyengar, S.S.; Tomasi, J.; Barone, V.; Mennucci, B.; Cossi, M.; Scalmani, G.; Rega, N.; Petersson, G.A.; Nakatsuji, H.; Hada, M.; Ehara, M.; Toyota, K.; Fukuda, R.; Hasegawa, J.; Ishida, M.; Nakajima, T.; Honda, Y.; Kitao, O.; Nakai, H.; Klene, M.; Li, X.; Knox, J.E.; Hratchian, H.P.; Cross, J.B.; Bakken, V.; Adamo, C.; Jaramillo, J.; Gomperts, R.; Stratmann, R.E.; Yazyev, O.; Austin, A.J.; Cammi, R.; Pomelli, C.; Ochterski, J.W.; Ayala, P.Y.; Morokuma, K.; Voth, G.A.; Salvador, P.; Dannenberg, J.J.; Zakrzewski, V.G.; Dapprich, S.; Daniels, A.D.; Strain, M.C.; Farkas, O.; Malick, D.K.; Rabuck, A.D.; Raghavachari, K.; Foresman, J.B.; Ortiz, J.V.; Cui, Q.; Baboul, A.G.; Clifford, S.; Cioslowski, J.; Stefanov, B.B.; Liu, G.; Liashenko, A.; Piskorz, P.; Komaromi, I.; Martin, R.L.; Fox, D.J.; Keith, T.; Laham, A.; Peng, C.Y.; Nanayakkara, A.; Challacombe, M.; Gill, P.M.W.; Johnson, B.; Chen, W.; Wong, M.W.; Gonzalez, C.; Pople, J.A. Gaussian, Wallingford CT, Gaussian 03, 2004. http://www.gaussian.com/g_misc/g03/citation_g03.htm
- (46) Jo, S.; Kim, T.; Iyer, V.G.; Im, W. *J. Comput. Chem.* **2008**, *29*, 1859–1865.
- (47) Martínez, L.; Andrade, R.; Birgin, E.G.; Martínez, J.M. *J. Comput. Chem.* **2009**, *30*, 2157–2164.
- (48) Phillips, J.C.; Braun, R.; Wang, W.; Gumbart, J.; Tajkhorshid, E.; Villa, E.; Chipot, C.; Skeel, R.D.; Kalé, L.; Schulten, K. *J. Comput. Chem.* **2005**, *26*, 1781–1802.
- (49) Huang, J.; MacKerell, A.D. *J. Comput. Chem.* **2013**, *34*, 2135–2145.
- (50) Jorgensen, W.L.; Chandrasekhar, J.; Madura, J.D.; Impey, R.W.; Klein, M.L. *J. Chem. Phys.* **1983**, *79*, 926–935.
- (51) Durell, S.R.; Brooks, B.R.; Ben-Naim, A. *J. Phys. Chem.* **1994**, *98*, 2198–2202.
- (52) Darden, T.; York, D.; Pedersen, L. *J. Chem. Phys.* **1993**, *98*, 10089–10092.
- (53) Essmann, U.; Perera, L.; Berkowitz, M.L.; Darden, T.; Lee, H.; Pedersen, L.G. *J. Chem. Phys.* **1995**, *103*, 8577–8593.
- (54) Miyamoto, S.; Kollman, P.A. *J. Comput. Chem.* **1992**, *13*, 952–962.
- (55) Ryckaert, J.-P.; Ciccotti, G.; Berendsen, H.J.C. *J. Comput. Phys.* **1977**, *23*, 327–341.
- (56) Grimme, S. *J. Comput. Chem.* **2006**, *27*, 1787–1799.
- (57) Weigend, F.; Ahlrichs, R. *Phys. Chem. Chem. Phys.* **2005**, *7*, 3297–3305.
- (58) Neese, F. *Wires. Comput. Mol. Sci.* **2012**, *2*, 73–78.
- (59) Grimme, S. *Wires. Comput. Mol. Sci.* **2011**, *1*, 211–228.
- (60) Grimme, S.; Antony, J.; Ehrlich, S.; Krieg, H. *J. Chem. Phys.* **2010**, *132*, 154104-1–154104-19
- (61) Becke, A.D.; Johnson, E.R. *J. Chem. Phys.* **2005**, *123*, 154101-1–154101-9
- (62) Neese, F.; Wennmohs, F.; Hansen, A.; Becker, U. *Chem. Phys.* **2009**, *356*, 98–109.
- (63) Grimme, S.; Ehrlich, S.; Goerigk, L. *J. Comput. Chem.* **2011**, *32*, 1456–1465.